CHAPTER FOUR

Depth-Dependent Lithospheric Stretching at Rifted Continental Margins

Mark Davis and Nick Kusznir

Introduction

While the uniform stretching model (McKenzie 1978) and its derivatives have been applied with considerable success to the formation of intracontinental rift basins, the mechanism for the formation of rifted continental margins is at best controversial. Rifted margins have traditionally been assumed to form by extreme extension and thinning of continental lithosphere (Le Pichon and Sibuet 1981), ultimately leading to the initiation of seafloor spreading at high stretching factor. Recent work on the northwest Australian rifted continental margin (Driscoll and Karner 1998; Baxter et al. 1999) and the Norwegian rifted continental margin (Roberts et al. 1997) suggests that the stretching of the continental lithosphere adjacent to the continent-ocean transition zone is highly depth dependent and increases with depth. The observation of depth-dependent lithosphere stretching at rifted margins is at variance with observations for intracontinental rift basins (White 1990; Marsden et al. 1990; Roberts et al. 1993), where stretching estimates derived from upper-crustal faulting balances that predicted for the whole lithosphere from postrift subsidence analysis, as predicted by McKenzie (1978). The stretching of the upper crust at rifted margins (Driscoll and Karner 1998; Baxter et al. 1999; Roberts et al. 1997) is observed to be significantly less than that of the whole crust or lithosphere, so that in the context of a simple-shear lithosphere extension detachment model (Wernicke 1985; Lister et al. 1991), all rifted continental margins appear to correspond to "upper plate." This observation has been named the "upper-plate paradox" by Driscoll and Karner (1998). Other recent work suggests that there is heterogeneous stretching on some rifted continental margins so extreme that it leads to the exhumation of mantle rocks. Wide regions of exhumed continental mantle of (up to ~100 km in width) have been observed at nonvolcanic rifted continental margins lying between the rotated fault blocks of highly extended continental crust and unequivocal oceanic crust (Pickup et al. 1996; Discovery 215 Working Group 1998; Whitmarsh et al. 2001). Observations of mantle exhumation are supported by wide-angle seismology, direct sampling,

geochemical analysis, magnetic anomalies analysis, and geological mapping of orogenically exhumed rifted margins.

Existing models of the formation of rifted continental margin fail to explain the observations of depth-dependent stretching and continental mantle exhumation at rifted continental margins. Given the fundamental importance of rifted continental margins in the plate-tectonic cycle and the advent of deep-water hydrocarbon exploration, it is important that the processes responsible for the formation of rifted continental margins are better understood. The objectives of this chapter are to describe new evidence for depth-dependent stretching at rifted continental margins from the analysis of data for the Goban Spur, Galicia Bank, Vøring, and South China Sea continental margins. In addition the mechanism of depth-dependent stretching and mantle exhumation is explored using simple analytical and finite-element fluid-flow models of the effect of early seafloor spreading on the adjacent continental margin lithosphere. A possible resolution of the "upper-plate paradox" identified by Driscoll and Karner (1998) is also examined.

Methodology for Determining Stretching Factors at Rifted Continental Margins

Three independent methods and data sets (figure 4.1) have been used to determine lithospheric stretching factors data for the Goban Spur, Galicia Bank, Vøring, and South China Sea continental margins. Upper-crustal extension has been calculated by summing the heaves measured on seismically imaged faults. Whole-crustal stretching is derived from crustal-thinning profiles constrained by seismic refraction, seismic reflection, or gravity inversion. "Whole-lithosphere" stretching has been determined from postbreakup thermal subsidence using flexural backstripping, decompaction, and reverse thermal subsidence modeling.

Upper-Crustal Stretching and Thinning

Extension in the brittle upper crust is derived from offsets on basement faults imaged on two-dimensional seismic reflection sections. Faults are assumed to be planar,

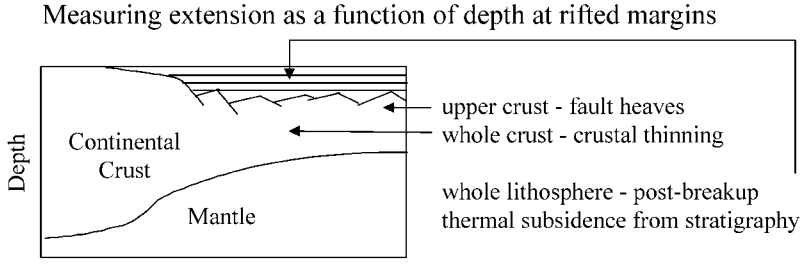

Figure 4.1 Schematic diagram illustrating the three independent methods used to independently estimate extension and stretching at depth within the lithosphere.

Table 4.1 Table of Parameters

Symbol	Quantity	Value	Units
β	stretching factor		—
β_a	apparent stretching factor		—
β_r	real stretching factor		—
ε	thinning factor		—
ε_{uc}	upper crustal thinning factor		—
ε_{lc}	lower crustal thinning factor		—
ε_{ml}	mantle lithosphere thinning factor		—
f	1 + fault underestimation factor		—
α	bedding rotation		°
θ	fault plane angle		°
l	horizontal fault offset		m
E	extension		m
v	vertical offset		m
W	distributed pure shear width	100	km
x	horizontal co-ordinate		km
x_0	fault location co-ordinate		km
t_0	initial crustal thickness	32	km

although extension estimates are not significantly altered if this assumption is invalid because the fault angle changes little over the measured vertical offset (see later discussion). Extension on a single fault (E_i) is given by simple trigonometry:

$$E_i = \frac{v_i}{\tan \theta_i} - l_i(1 - \cos \alpha_i) \tag{4.1}$$

where E is extension, v is the vertical offset between footwall and hangingwall fault cutoffs, θ is fault dip, and l is the horizontal separation (see table 4.1 for a full definition of terms). Measured vertical offsets are used to generate fault heaves (through assumed dips on the fault plane), because they are measured more reliably than horizontal fault offsets. True dip section profiles are used, although since only the dip-slip component of faults contributes to crustal thinning, faults with slip directions that are not coincident with the two-dimensional depth profiles do not influence our analysis. We choose to ignore the block rotation component because several studies have demonstrated that faults are more likely to deform by vertical shear than as rigid "dominoes" (Westaway and Kusznir 1993). By making this assumption, we may slightly *overestimate* fault-related extension. To capture the error and uncertainty inherent in deriving stretching factors from faults, we vary the present-day fault dip θ from 25 to 70° for each fault.

It is convenient to define the 'thinning' factor, which is related to the stretching factor by equation (4.2).

$$\varepsilon = 1 - \frac{1}{\beta(x)} \tag{4.2}$$

S
N
L

To compare upper-crustal stretching with similar estimates for the whole crust and "whole lithosphere," we express fault-derived extension (measured discretely from faults) as a laterally varying profile of stretching factor β. In the reference frame of the extended continental lithosphere, extension is derived from β by

$$E = \int \varepsilon dx = \int \left(1 - \frac{1}{\beta(x)}\right) \mathrm{d}x \tag{4.3}$$

Extension from a single fault is mapped to a profile of stretching factor using a continuous function such that the distributed extension is identical to that measured discretely on faults. The form and width of the function that maps fault-derived strain to a continuous function is arbitrary (White and McKenzie [1988] use a Gaussian function) but not critical, because neither assumption alters the total extension. We choose to use a cosine-squared function, which is continuous and has continuous first derivatives:

$$\beta_{\mathrm{i}} = 1 + \beta_0 \cos^2 \left[\frac{\pi(x - x_0)}{W}\right] \tag{4.4}$$

In the stretched reference frame, extension is given by equation (4.5), where the value of β_0 is determined numerically:

$$E = \int \left[1 - \frac{1}{\beta}\right] \mathrm{d}x = \int \left[1 - \frac{1}{\beta_0 \cos^2 \left[\frac{\pi(x - x_0)}{W}\right]}\right] \mathrm{d}x \tag{4.5}$$

The total stretching factor (β_{tot}) associated with all faults is the product of stretching-factor profiles associated with each fault. Values of W in the range 75 to 150 km have been used (Roberts et al. 1993).

Whole Crustal Stretching and Thinning

Crustal thickness variation along rifted continental margins is assumed to be the consequence of crustal extension and thinning and is used to infer the lateral distribution of strain. Crustal thickness is derived from wide-angle seismic studies; where these are unavailable, the "reflection Moho" or data from gravity studies are used. Assuming a constant initial crustal thickness (t_0), the crustal-derived stretching factor is

$$\beta = \frac{t_0}{t_{\mathrm{c}}} \tag{4.6}$$

S
N
L

In our analysis we generally assume that the crustal thickness variations are due to stretching during the event under study. Where this assumption is clearly invalid (e.g., along the Norwegian margin that has a long tectonic history of lithosphere extension), instead of controversially attempting to partition crustal-thickness variations to separate events, we consider these data to be unreliable and hence do not use them in our analysis. The assumed initial crustal thickness is constrained where possible with local data, and we capture the associated likely uncertainty in the calculation of error bars in stretching and thinning factors (see later discussion).

Whole Lithosphere Stretching and Thinning

Reequilibration of lithosphere temperature anomalies generated during lithosphere stretching gives rise to postrift "thermal" subsidence (McKenzie 1978). The postbreakup subsidence history of a rifted margin recorded in stratigraphic data contains information that allows the magnitude of lithosphere stretching to be determined. Two-dimensional flexural backstripping, decompaction, and reverse postbreakup thermal subsidence modeling has been applied to two-dimensional depth converted stratigraphic cross sections derived from seismic reflection data to determine "whole lithosphere" stretching factors. The methodology is described in Roberts et al. (1998). The flexural backstripping, decompaction, and reverse postbreakup thermal subsidence modeling takes a present-day section and produces a series of palaeo cross sections whose palaeobathymetries are dependent on the magnitude of the lithosphere-stretching factor (McKenzie 1978) used in the reverse postbreakup thermal modeling. Calibration of the palaeo cross sections by observed palaeobathymetry indicators allows the magnitude and lateral variation of lithosphere-stretching factor to be determined. Throughout this chapter we compute equivalent "whole lithosphere" stretching factors using the assumption of uniform stretching. Where depth-dependent stretching occurs, the "true" lithospheric mantle-stretching factor may be greater than the equivalent "whole lithosphere" stretching factor, as enhanced stretching in the lithospheric mantle is required to offset suppressed crustal extension.

Stretching Observations on the Goban Spur Rifted Margin (UK Margin)

The Goban Spur rifted continental margin lies off southwest England (figure 4.2a). The margin lies in deep water and was formed by lithospheric extension as separation occurred between Europe and North America from the early Cretaceous to mid-Albian (Masson et al. 1985; de Graciansky and Poag 1985). In this analysis the structure of the margin is assumed to be two-dimensional, which is probably a reasonable approximation because major lateral changes in margin morphology occur on length scales greater than 100 km (Horsefield et al. 1993). Figure 4.2b–d illustrates line drawings of the interpretations of seismic reflection profile data at Goban

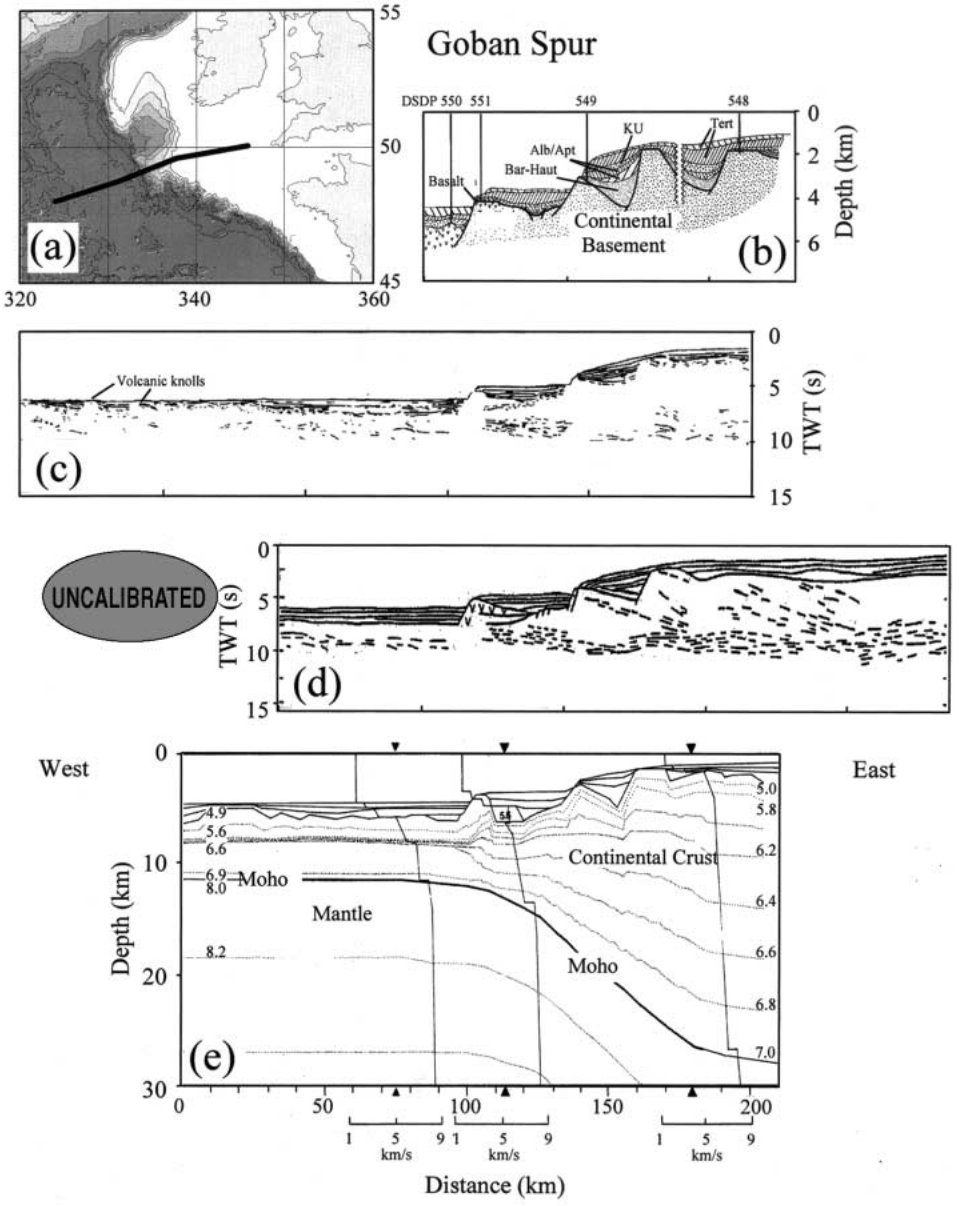

Figure 4.2 (a) Bathymetry at the Goban Spur rifted continental margin showing location of the profile used in this study. (b) Illustration of the interpreted depth section at Goban Spur, interpreted from seismic line CM10, and reproduced after (de Graciansky et al. 1985). (c and d) Line drawings of the outer section of BIRPS WAM line (Klemperer and Hobbs 1989; Peddy et al. 1989; Louvel et al. 1997). (d) Line drawing of BIRPS deep-seismic profile WAM. (e) Crustal structure and velocity structure at Goban Spur from seismic refraction data (Horsefield et al. 1993). The conventional "continent-ocean boundary" is usually interpreted to be coincident with DSDP Site 551. The reflection Moho in the interpreted oceanic domain is associated with very few identifiable reflectors. Black circles indicate two volcanic knolls.

S
N
L

Spur (de Graciansky and Poag 1985; Klemperer and Hobbs 1991; Louvel et al. 1997). The outer margin consists of a series of rotated basement-fault blocks that are clearly imaged on seismic reflection because of the relative lack of sedimentary cover. Rifting at the Goban Spur margin has had a long history. Permo-Triassic and Jurassic basins lie to the east of the continent-ocean boundary (Cook 1987), and the age of the structures generally young to the west. A Jurassic rift system manifested by northeast-southwest trending faults has been overprinted in the west, within ~100 km of the "continent-ocean boundary," by Cretaceous northwest-southeast trending faults. The age of the latest rift event that leads to continental breakup is constrained by DSDP wells to be in the Albian-Aptian interval (105–112 Ma; Joppen and White 1990), and the oldest seafloor magnetic anomaly is M34 (Albian-Santonian; Scrutton 1984). The seismic reflection line drawing shown in figure 4.2b taken from de Graciansky and Poag (1985) shows pre-, syn-, and postbreakup stratigraphy and clear breakup age upper-crustal faulting.

Deep normal incidence seismic reflection profiles from the WAM survey at Goban Spur (Peddy et al. 1989; Klemperer and Hobbs 1991; Louvel et al. 1997) reveal that the upper crust is relatively transparent and the lower crust is reflective (figure 4.2c and d), and as such, Goban Spur is typical of many deep-seismic reflection sections from around the British Isles (Cheadle et al. 1987). While the origins of the reflectivity are debated (Mooney and Meissner 1992), the base of the lower-crustal reflective zone is approximately coincident with the seismic refraction Moho and is therefore usually interpreted to represent the "seismic reflection" Moho. The results of refraction seismology work at Goban Spur (figure 4.2e) by Horsefield et al. (1993) confirms that the base of the lower-crustal reflective zone corresponds to the Moho for Goban Spur. Peddy et al. (1989) note that the reflective lower crust appears to thin in proportion to the whole crust. They suggest that lower-crustal reflectivity is a prerift feature and that extension of the lithosphere is consistent with uniform pure-shear (McKenzie 1978).

The conventional continent-ocean boundary is usually interpreted to be the volcanic knoll sampled by DSDP Site 551 (figure 4.2b–d). The "oceanic crust" to the southwest of the continent-ocean boundary is characterized by an irregular surface with little evidence of a reflection Moho. Goban Spur is often cited as a classic "nonvolcanic" margin (Watts and Fairhead 1997). Wide-angle seismic studies (Horsefield et al. 1993; figure 4.2e) provide no evidence for the high-velocity lower crust (V_p = 7.2–7.4 km s^{-1}) which would be diagnostic of basaltic underplating commonly found at "volcanic" rifted continental margins. Furthermore, Horsefield et al. (1993) and Masson et al. (1985) support the notion that (a) typical oceanic crust lies westward of a narrow (~15 km) continent-ocean boundary and that (b) there is *no evidence for depth-dependent stretching* (Horsefield et al. 1993). More recent work (Minshull et al. 1998), involving both reinterpretation of existing data and new data, challenges these notions. We suggest that the intracrustal velocity structure is not sufficiently unique to enable determination of intracrustal stretching factors; indeed, much of the internal structure may be an artifact of the modeling technique. Seismic reflection reveals (figure 4.2c) that the conventional

S
N
L

oceanic crust at Goban Spur is characterized by an irregular surface and shows little evidence of a reflection Moho. It may be that unequivocal oceanic crust lies immediately to the southwest of the two prominent ridges located close to the western end of the WAM profile (Klemperer and Hobbs 1991; figure 4.2c), with transitional material to the landward side. The original seismic data (not reproduced here) reveals a strong reflector at ~1.3 s two-way time below the top of the (presumed) oceanic crust. This may suggest that this location is the "true" continent-ocean boundary and that the poor fitting of the amplitudes of P_n arrivals from the wide-angle data set (Horsefield et al. 1993) at Goban Spur does not provide strong support for a well defined and abrupt continent-ocean boundary.

Fault Extension Stretching Factors

The analysis of upper-crustal faulting was made from an interpretation largely derived from the deep-seismic reflection profile WAM (Klemperer and Hobbs 1991; figure 4.2c and d) and published sections of the higher-resolution data sets (CM-10 from de Graciansky and Poag 1985; figure 4.2b), with stratigraphic calibration and depth-conversion information from DSDP reports (Masson et al. 1985). Note that the sections interpreted from the WAM deep-seismic line (figure 4.2c and d) and the higher-resolution line CM-10 (figure 4.2b) are similar and image few upper-crustal faults. Total extension estimates for the outer ~100 km (the region corresponding to the wide-angle survey shown in figure 4.2e) is 12 ± 5 km, or $\beta = 1.13 \pm 0.05$. The error estimate assumes the uncertainty in estimating fault dip is $\pm 10°$. Present-day fault dips range from 35° to 70°, but the "average" observed dip is ~55°. The lateral profile of stretching and thinning factors derived from the upper crust is illustrated in figure 4.3a and b.

Crustal Thinning Stretching Factors

The crustal structure used to determine crustal thinning stretching factors is summarized in figure 4.3c and is derived from wide-angle refraction results taken from Horsefield et al. (1993), and shown in figure 4.2e, and depth-converted normal incidence deep-seismic data (Klemperer and Hobbs 1991). There is generally good agreement (<2 km misfit) between the reflection and refraction estimates of the seismic Moho. The crustal stretching (β) and thinning (ε) factors are calculated assuming an initial homogenous prerift crustal thickness of 32 ± 2 km (Bott and Watts 1970).

Figure 4.3a and b shows the profiles of crustal thinning-derived stretching and thinning factors. Errors in stretching factor (β) have been calculated assuming uncertainties of $\pm 1/2$, ± 2 km, and ± 2 km for top basement, Moho (Horsefield et al. 1993), and prerift (homogenous) crustal thickness, respectively. While errors in the thinning factor (ε) are symmetric, errors in the associated stretching factor

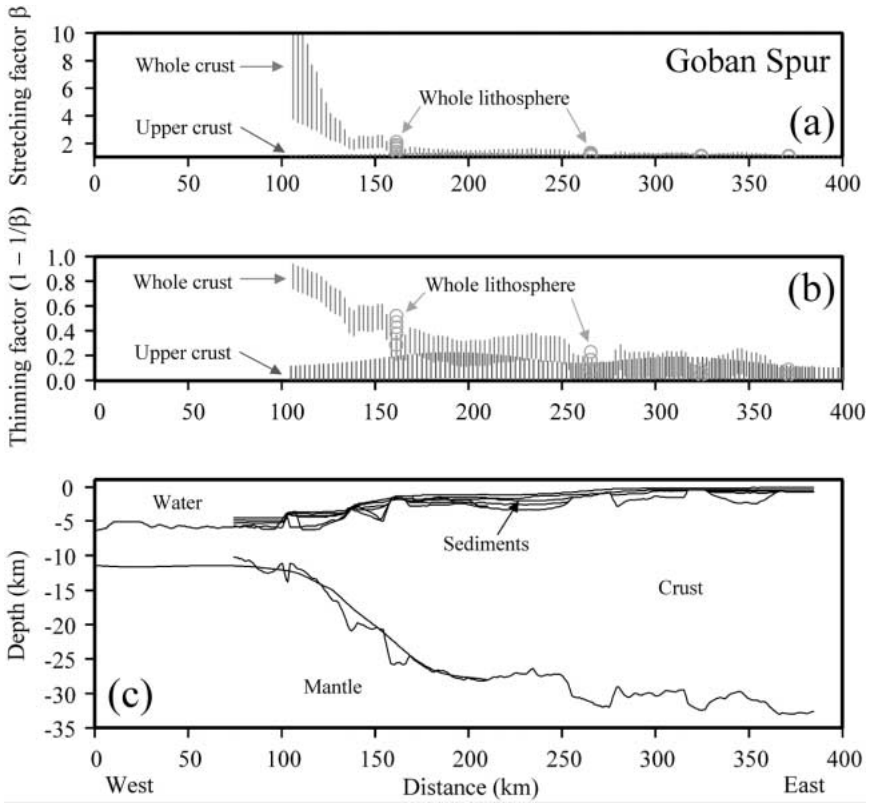

Figure 4.3 (a and b) Stretching and thinning factors for upper crust, whole crust, and "whole-lithosphere" for the Goban Spur rifted margin. Circles represent estimates of "whole-lithosphere" stretching factors with effective elastic thicknesses (T_e) of 0, 3, 5, 10 km. Whilst stretching estimates are similar toward the continental interior, a significant discrepancy is evident within ~75 km of the continent-ocean boundary. (c) Crustal sections derived from seismic data summarized in figure 4.2. Vertical lines of stretching and thinning factor derived from upper-crustal faulting and crustal thinning represent error bars of ±1.5 standard deviation.

(β) are not. The crustal thinning-derived extension estimate is 42 ± 8 km, or in terms of mean stretching factor, $\beta = 1.7 \pm 0.25$.

"Whole-Lithosphere" Stretching Factors

Flexural backstripping, decompaction, and reverse postbreakup thermal subsidence modeling has been carried out at Goban Spur to determine "whole-lithosphere" stretching factors. The present day two-dimensional stratigraphic cross sections used as input to the flexural backstripping, decompaction and reverse postbreakup thermal subsidence modeling were derived from the WAM seismic reflection profile (Klemperer and Hobbs 1991) and published sections of the higher-resolution CM-

10 data set (de Graciansky and Poag 1985), with stratigraphic calibration and depth-conversion information from DSDP reports (Masson et al. 1985). The depth-converted stratigraphy is summarized in figure 4.3c. As seen on seismic reflection data for Goban Spur (de Graciansky and Poag 1985; Klemperer and Hobbs 1991; Louvel et al. 1997) and summarized in figure 4. 2b–d, several of the fault blocks have bevelled tops that have been eroded at or near sea level. These eroded fault blocks are believed to be reliable palaeobathymetric markers and are therefore used to constrain our reverse postbreakup thermal subsidence modeling. Compaction parameters from Sclater and Christie (1980) have been used, and the pre-, syn-, and postbreakup lithologies are taken to be sandy-shale and chalk, respectively. An instantaneous rift age of 105 Ma is assumed and has been used to define the post-breakup thermal subsidence. To simulate the thermal load from adjacent oceanic crust, the stretching-factor profile has been ramped to $\beta = \infty$ at the conventional continent-ocean boundary (at ~100 km on figure 4.3c).

The estimates of lithosphere stretching and thinning factor derived from flexural backstripping, decompaction, and reverse thermal subsidence modeling are shown in figure 4.3a and b. The lateral coupling of the adjacent oceanic thermal load into the rifted continental margin region is a strong function of the assumed effective elastic thickness (T_e) used in the flexural backstripping, decompaction, and reverse thermal subsidence modeling. As a consequence, the modeling has been performed with values of $T_e = 0$, 3, 5, 10, 25 km to determine sensitivity to T_e. No eustatic sea level curves are applied, because their timing and magnitude are debated (Hall and White 1994). By ignoring possible eustatic sea level change (which may have been up to ~300 m higher 70 Ma BP; Pitman 1978), the β factor is potentially underestimated by $\Delta\beta$ ~0.2.

Stretching Factor Variation with Depth on the Goban Spur Rifted Margin

Figure 4.3a and b shows the lateral profiles of stretching factor along the Goban Spur margin where fault and crustal thinning derived estimates are shown with their appropriate error bars, and backstripping-derived estimates of " whole-lithosphere" extension are marked with circles at locations with good palaeobathymetric control. The clusters of β estimates from flexural backstripping span the likely bounds of lithospheric effective elastic thickness (T_e) as described in a previous section. While the spectral signature of the sediment is dominated by long wavelengths, the short wavelength of the thermal load associated with the adjacent oceanic crust generates a strong dependence of the stretching factor to the lithosphere effective elastic thickness. As figure 4.3b illustrates, the "whole-lithosphere" stretching factor is significantly greater (i.e., without the error bars) than upper-crustal stretching factors for all values of effective elastic thickness (T_e). The figure demonstrates that there appears to be no significant increase in the upper-crustal stretching factor toward the continent-ocean boundary, and suggests that depth-dependent stretching occurs within ~75 km of new oceanic crust.

S
N
L

Stretching Observations on the Galicia Bank Rifted Margin (Iberian Margin)

The rifted continental margin off the west coast of Iberia (figure 4.4a) is a "non-volcanic" margin and formed during the continental separation between Iberia and Newfoundland that led to the opening of the North Atlantic ocean. The margin developed during a Berriasian/latest Aptian rifting episode (140–114 Ma; Boillot et al. 1989b), and is conjugate to the southeast Flemish Cap margin. While the margin has small free-air gravity anomalies (Sandwell and Smith 1997) and is approximately in isostatic equilibrium, the free-air edge-effect couplet typical of the continent-ocean boundary in many regions appears to be absent or suppressed. Oceanward of the narrow shelf lies the Galicia Interior Basin, which is probably a continuation of the Lusitania Basin of onshore Portugal. The Galicia Interior Basin suffered several episodes of rifting from Triassic to early Cretaceous and proceeded to break up to the west some 25 Ma later (Perez-Gussinye et al. 1998).

The outer margin comprises a series of rotated fault blocks striking north, dipping both to the east and west in the east and mainly to the west in the west (figure 4.4b; Whitmarsh et al. 1996). Fault blocks in the extreme west, near to the postulated continent-ocean boundary, are remarkable in that they have little or no postbreakup sedimentary cover (figures 4.4b and 4.5a). Normal incidence reflection data at the Galicia margin indicates the presence of a strong midcrustal (so-called S-) reflector which is continuous and almost linear over the outer 50 km of the margin (figure 4.5b; Reston 1996). While for many years the origin of the

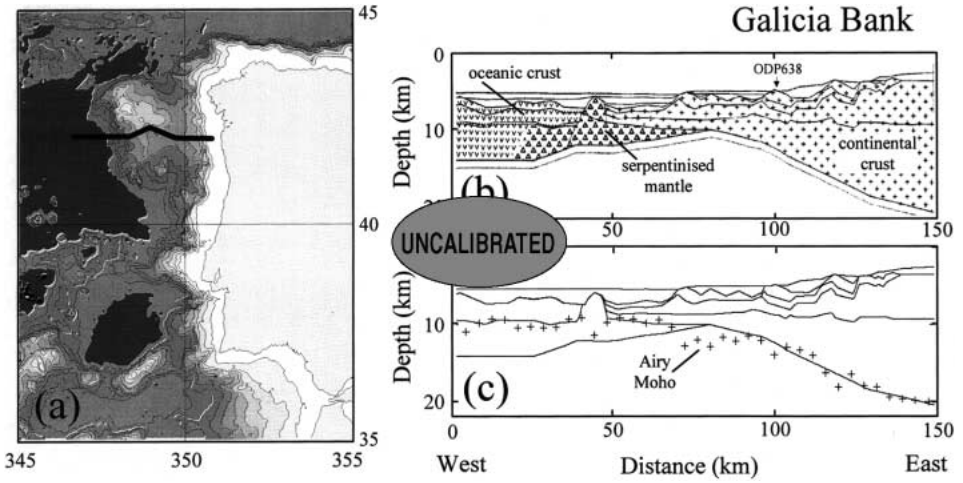

Figure 4.4 (a) Location map showing bathymetry offshore Portugal and the location of the Galicia Bank profile used in this study. (b) Crustal model derived from wide-angle data after Whitmarsh et al. (1996). (c) Wide-angle data set with estimates of the depth to Moho (asterisks) from an Airy-isostatic model. The small misfit between independent models provides confirmation that the margin is presently at or close to Airy isostatic equilibrium, a point that is discussed later.

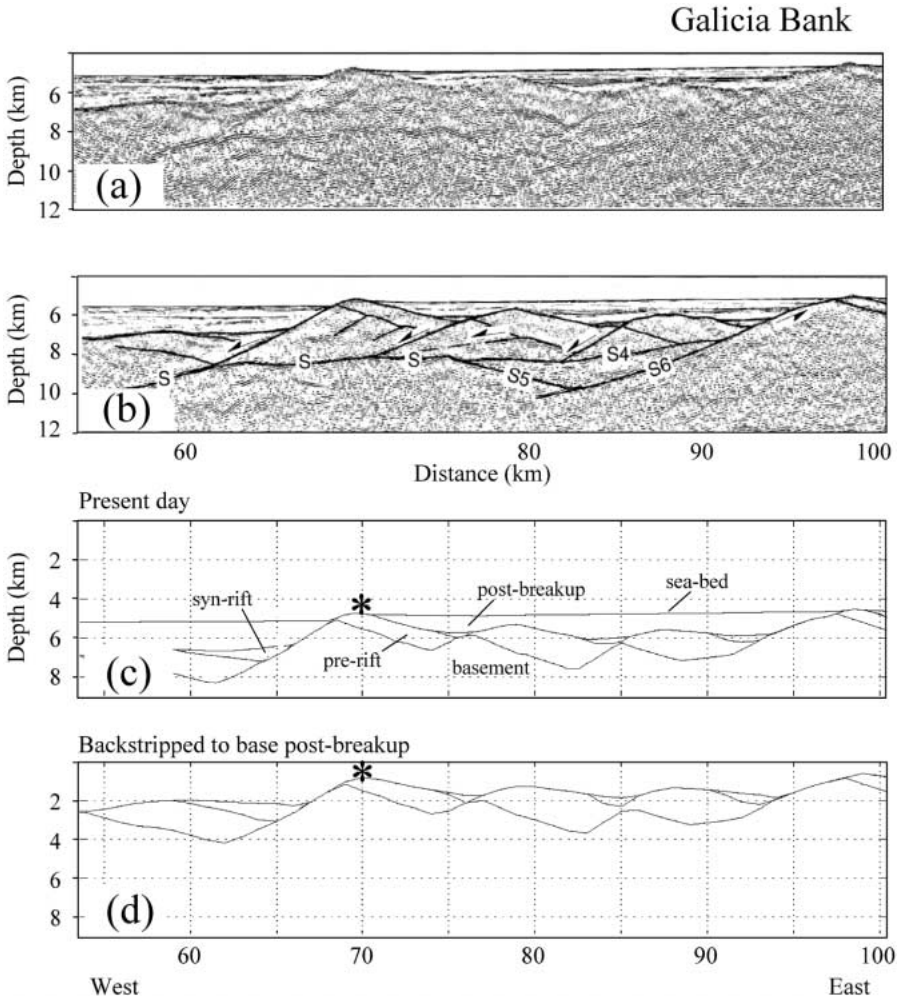

Figure 4.5 (a and b) Depth-migrated seismic reflection section and interpretation for Galicia Bank. (c) Present-day depth cross section; asterisk denotes fault block crest possibly beveled by erosion at or near sea level. (d) Depth cross section restored to base breakup using flexural backstripping and reverse postbreakup thermal subsidence with a β factor of infinity.

S-reflector was highly controversial, waveform modeling (Reston 1996; Whitmarsh et al. 1996) strongly suggests that the S-reflector represents a major detachment fault with a top-to-the-west sense of shear, a notion that is supported by similar "D" reflectors on the southern Iberian Abyssal Plain margin (Pickup et al. 1996). The Iberian margin shows a major detachment feature as predicted by a Wernicke-type simple-shear model (Wernicke 1985; Lister et al. 1991).

Figure 4.4b summarizes the wide-angle velocity model for the northern Galicia margin (Whitmarsh et al. 1996). The Moho in the west is overlain by a lens of high-velocity material, for which there are two explanations, namely: (a) ser-

S
N
L

pentinized peridotite, or; (b) igneous underplating. P_mP arrivals were not observed at the west end of the refraction line, which suggests that velocity contrast is small. Since there is very little evidence of syn-rift melt (Whitmarsh et al. 2001) as is typical of "volcanic" margins (White and McKenzie 1989), the serpentinzation model is preferred. Figure 4.4c shows (with asterisks) a Moho predicted by Airy isostasy superimposed on the crustal structure derived from wide-angle seismology shown in figure 4.4b (Whitmarsh et al. 1996). The agreement between the seismic Moho (figure 4.4b) and Airy isostatic Moho (figure 4.4c) suggests the margin is in near local isostatic equilibrium.

A composite regional two-dimensional reflection profile has been generated by compiling four published seismic reflection sections. Seismic lines GAP-106 and GAP-014 splice to the regional wide-angle model, which in turn is coincident with reflection line segment GP-101. Depth conversion of the eastern portion of the composite reflection seismic was performed using velocities described in Murillas et al. (1990). This composite section is not reproduced to conserve space, although a simplified line drawing is shown in figure 4.6c.

Fault-Derived Stretching Factors

The determination of upper-crustal extension was made from the analysis of upper-crustal faulting observed on the composite section described previously. The analysis used 35 seismically observable faults using the methodology described under Methodology for Determining Stretching Factors at Rifted Continental Margins. Total recorded extension on this profile is 80 $\pm$ 12 km giving an equivalent mean stretching factor $\beta = 1.3 \pm 0.1$. The lateral profile of stretching and thinning factors derived from the upper crust is illustrated in figure 4.6a and b.

Crustal Thinning Stretching Factors

To extend our knowledge of depth to Moho eastward of that observed seismically on the margin, Moho depth has been determined from inversion of gravity anomalies, constrained by sediment thickness and bathymetry data. Where overlap with seismically determined Moho depth occurs, the Moho derived from Bouguer gravity inversion and wide-angle refraction are consistent and have misfits typically $<$1 km (figure 4.6c). Crustal thickness has been determined using the methodology outlined under Whole Crustal Stretching and Thinning from the crustal structure-thickness profile shown in figure 4.6c. An initial crustal thickness of 30 km was used consistent with the crustal-thickness estimates from unstretched crustal thickness under Iberia (Cordoba et al. 1987) and the Airy Moho depth (figure 4.4c). The resulting profile of stretching and thinning factors derived from crustal thinning is shown in figure 4.6a and b.

Errors in stretching factor (β) have been calculated assuming uncertainties of ± 1, ± 2, and ± 2 km for top basement, Moho, and prerift (homogenous) crustal

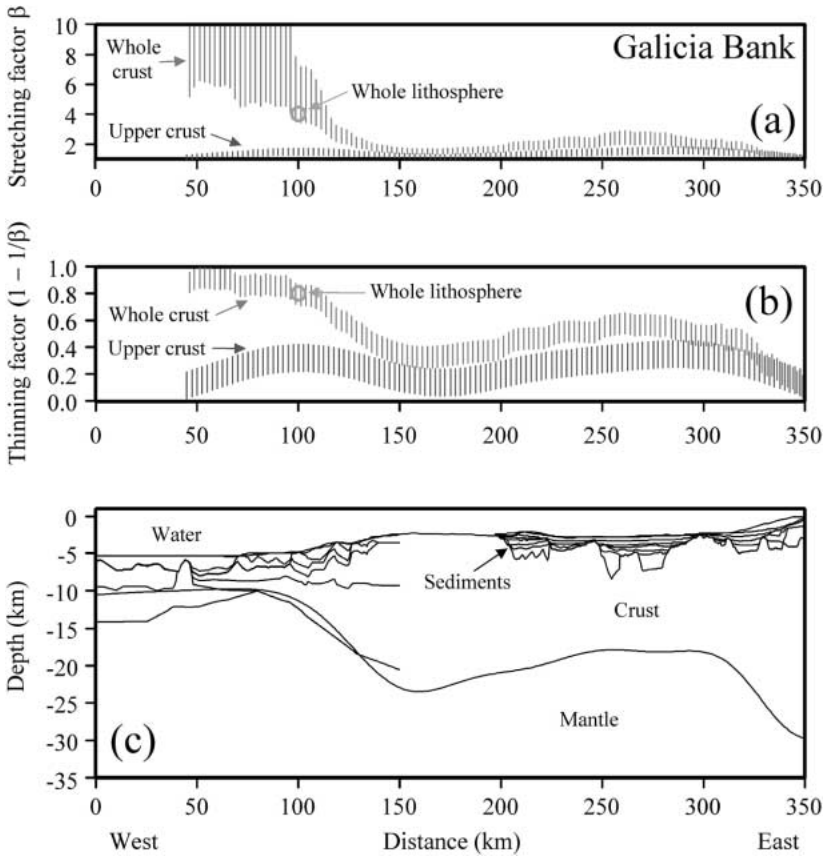

Figure 4.6 (a and b) Stretching and thinning factors for the upper crust and whole crust at the Galicia Bank rifted continental margin. The open circle at coordinate ~100 km is an estimate of whole-lithosphere stretching from Airy backstripping. (c) Crustal section derived from seismic and gravity.

thickness, respectively. Crustal-derived extension at Galicia is 203 ± 37 km giving an equivalent mean stretching factor $\beta = 2.9 + 1.5/-0.7$. Note that the errors are significantly asymmetric at large stretching factors.

Stretching Factor Variation with Depth on the Galicia Bank Rifted Margin

Stretching and thinning factors for the upper crust and whole crust are compared in figure 4.6a and b and are significantly different within ~130 km from the end of the composite profile, or ~75 km from the conventional continent-ocean boundary. This difference has been noted before (Boillot et al. 1989a, 1989b; Chenet et al. 1982; Sibuet 1992).

"Whole-Lithosphere" Stretching Factors and Postbreakup Subsidence

Profile GP101 (figure 4.5a and b; Reston 1996), coincident with the outer part of our composite line (figure 4.6c), is remarkable in that the postrift sedimentary cover is thin (mostly <1 km), and most unusually, the fault block at $\sim$70 km has no postrift cover, presumably because the sediment supply was low and the spill point has never been reached. A simplified depth section of line GP101 is shown in figure 4.5c. The possibility exists (but it is by no means certain) that the beveled fault block identified with an asterisk at 70 km (figure 5c) represents a palaeobathymetric marker at or near sea level at the end of breakup. The results of restoring this section to base postbreakup (end breakup) using flexural backstripping, decompaction, and reverse thermal subsidence modeling with $\beta = \infty$ and $T_e = 3$ km is shown in figure 4.6d. Even with the largest stretching factor possible driving the postbreakup thermal subsidence ($\beta = \infty$), the beveled fault blocks fail to restore to sea level independently of the T_e used for the flexural response of the lithosphere.

Whilst high stretching factors are not unexpected because the section lies in water $\sim$5 km deep, the postrift thermal subsidence predicted by McKenzie (1978) only predicts $\sim$4 km after $\sim$150 Ma for a stretching factor $\beta = \infty$. Such anomalous subsidence is difficult to explain using conventional models and cannot be accounted for by eustatic sea level variation. Using an instantaneous rift age of 141 Ma (Whitmarsh et al. 1996) does little to change the palaeobathymetry predicted at the end of the syn rift, which is $>$750 m for the older rift age for $T_e = 3$ km and $\beta = \infty$. While it is uncertain whether the fault blocks were eroded at sea level, from what is known about the end syn-rift palaeobathymetries, such deep water is unlikely. Similarly, and as noted by Whitmarsh et al. (1996) and Louden et al. (1991), the stretching factor estimated from Airy backstripping of ODP sites 639, 640, and 641 (situated in shallower water to the east of GP101 and figure 4.5) is larger than that determined from faulting and fits either an instantaneous model $\beta\sim4$ or a finite-duration rift event of similar total magnitude. A "whole-lithosphere" stretching factor $\beta\sim4$ is consistent with the crustal-thinning estimate but is significantly greater than the fault-derived estimate.

Speculation on the Cause of Anomalous Subsidence on the Galicia Bank Margin

The observation that the northern Iberian rifted continental margin is in near local isostatic equilibrium and the initial crustal thickness was 30 ± 1 km suggests that the prerift margin should have been sufficiently buoyant to be at sea level before rifting. As noted in the previous section, the $\sim$5 km of water-loaded subsidence since breakup is greater than the thermal subsidence predicted by the uniform stretching model (McKenzie 1978), even for very large stretching factors (for $\beta = \infty$, only 4 km of subsidence is predicted since breakup). If the fault block was

at sea level at breakup then ~1 km of fault-block water-loaded subsidence of the present-day bathymetry may be derived from syn-breakup subsidence that occurred during sediment-starved conditions. Under traditional models of rifting this observation is most unusual because syn-rift footwall uplift on large faults is well documented (Stein and Barrientos 1985) and usually causes foot-wall erosion. The failure of the section to backstrip to sea level may therefore suggest that extension of the western Iberian lithosphere occurred in two phases driven by two dissimilar processes. A modest initial stretching phase (β ~1.3, say, consistent with the upper-crustal fault-derived extension estimate) may have generated the observed fault geometries. Subsequently, depth-dependent stretching of the lithosphere may have occurred within the ductile lower crust and lithospheric mantle and generated further syn-breakup subsidence by lower crustal thinning without additional footwall uplift. Such a two-phase stretching model may provide a general explanation for the observation of apparent depth-dependent stretching of the lithosphere at rifted continental margins and is discussed subsequently in more detail.

Stretching Observations on the Vøring Rifted Margin (Mid Norway Margin)

The Norwegian rifted continental margin (figure 4.7a) is the culmination of a complex history of extensional tectonics since the Devonian Caledonian orogeny (Gage and Dore 1986). The most recent extensional events were the late Jurassic-early Cretaceous intracontinental rift event and the Palaeocene rift event that immediately preceded the late Palaeocene-early Eocene breakup during isochron 24r at ~55 Ma (Eldholm et al. 1995). Given the complex stretching history along the Norwegian margin, in this chapter estimates of stretching factors are only calculated for the Palaeocene (and late Upper Cretaceous) stretching events immediately leading up to continental breakup and rifted margin formation at ~55 Ma. The central and outer parts of the Norwegian margin have large accumulations of sediment (figure 4.7b). While the stratigraphy in the east is constrained by published hydrocarbon exploration wells and shallow boreholes, the deep-water stratigraphy determined by recent commercial drilling remains largely confidential. Consequently the stratigraphy used in this study is largely derived from the predrilling interpretations provided by Statoil (and published in Dore et al. 1997). The deepest visible reflector is believed to be the base Cretaceous (Blystad et al. 1995) with maximum depth of ~12 km (~7 s two-way travel time) below the sea surface. With the exception of the vicinity of the conventional continent-ocean boundary, where extrusive volcanics limit seismic penetration, extensional structures of Palaeocene age are normally well imaged by normal-incidence seismic reflection profiles.

The Norwegian margin is characterized by large amounts of igneous volcanic activity and is classified as a "volcanic" margin to distinguish it from other "non-volcanic" margins such as Goban Spur and west Iberia (White and McKenzie

S
N
L

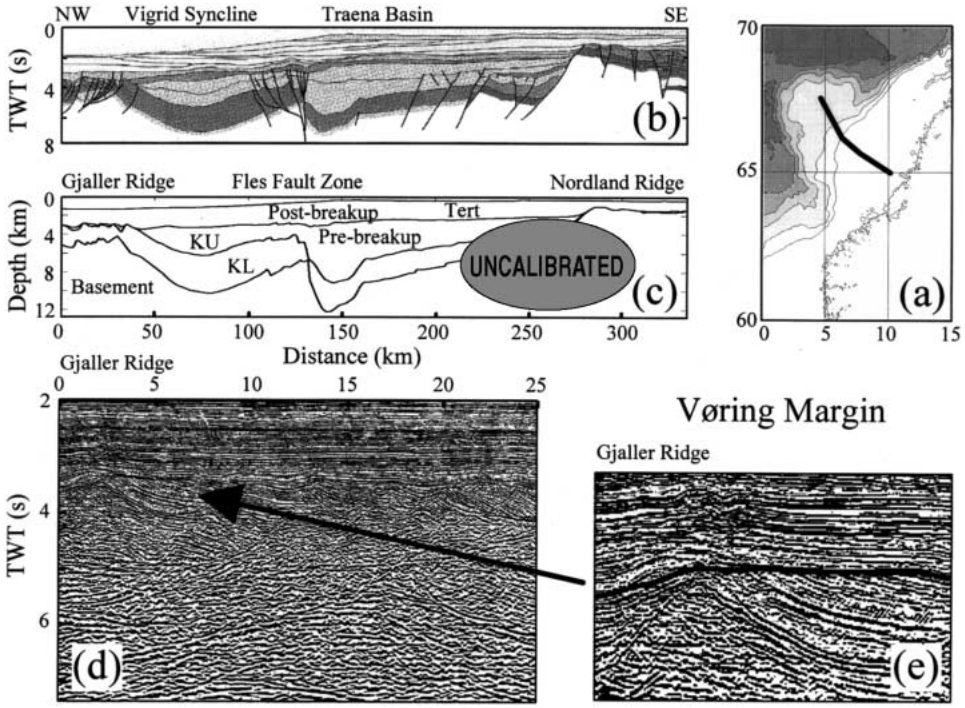

Figure 4.7 (a) Location map showing bathymetry offshore mid-Norway and the location of the Vøring Margin profile used in this study. (b and c) Depth and seismic reflection cross sections (e and f) for the Vøring Margin profile used in this study. Depth cross section and seismic data taken from Dore et al. (1997).

1989). The igneous activity at "volcanic" margins is evidenced by seaward dipping reflectors (SDRs), sill intrusions, high velocity and high density bodies with high MgO content, and extrusive lavas (White and McKenzie 1989). Close to the conventional continent-ocean boundary lies a significant "marginal high"—a feature common to many "volcanic" margins—which was formed during early Cenozoic rifting and breakup with emplacement of large volumes of igneous rocks, which were extruded at the surface and intruded as sills and underplating bodies (Mjelde et al. 1997a, 1997b). In this vicinity seaward-dipping reflectors are imaged on seismic reflection sections that were established by drilling (DSDP Leg 81 and ODP Legs 104, 152, and 163) to be T-MORB tholeiitic basalt lava flows extruded under subaerial or shallow marine conditions (Planke and Eldholm 1994). Pb-isotope studies of DSDP Leg 81 suggest that the extrusive lavas that form the seaward dipping reflectors are contaminated with a crustal signature (Morton and Taylor 1987) and therefore lie landward of the continent-ocean boundary, as proposed by Hinz (1981), in contrast to the subaerial seafloor spreading model of Mutter et al. (1982).

The Vøring basin (figure 4.7a) lies off the west coast of Norway at 66–68 °N. Figure 4.7b and c shows a section, taken from Line D of Dore et al. (1997), across

the Vøring basin running from the Nordland Ridge, over the Traena basin, the Vigrid Syncline, and Gjaller Ridge toward the Vøring Marginal High (not shown), which is close to the continent-ocean boundary. Age and lithology data derived from regional interpretations by Statoil tie into commercial well 6508/5–1 to the east of the Nordland Ridge. Time-depth functions for depth conversion of seismic reflection data (figure 7c) are derived from wells from the Magnus/Southern Møre Basin area.

The Gjaller Ridge (figure 7b–e) is a prominent northeast-southwest trending high comprising mainly westward-dipping, deeply eroded, rotated, mainly pre-Tertiary fault blocks (Dore and Lundin 1996; Blystad et al. 1995). This ridge has a well developed unconformity at the Base Tertiary (65 Ma) and deeply eroded Cretaceous fault blocks that result from end-Cretaceous extension and contemporaneous footwall uplift (figure 4.7d and e). The Gjaller Ridge, and similarly the Fles Fault Zone, are believed to have been at (or near) sea level in the Palaeocene so providing a palaeobathymetric constraint for flexural backstripping. In addition, the Vøring Marginal High to the west (not illustrated) is interpreted to be a regional (near) sea level marker at Top Palaeocene times (57 Ma) since DSDP and ODP drilling found basaltic lavas interbedded with shallow-marine sediments (Planke and Eldholm 1994).

Fault-Derived Stretching Factors

The analysis of upper-crustal faulting to determine Palaeocene (and late Upper Cretaceous) upper-crustal extension associated with continental breakup was made from the section shown in figure 4.7b and c and taken from Line D of Dore et al. (1997). The seismic data on which this interpretation by Dore et al. (1997) is based is of good quality and allows the identification of small extensional faults (figure 7d and e). Fault-derived stretching and thinning factors are shown in figure 4.8a and b. Upper-crustal stretching factors are small, peaking at $\beta \sim 1.1$ around the Gjaller Ridge. Total extension derived from Palaeocene faulting is 10 ± 4 km. The mean stretching factor from the Fles Fault Zone to the "continent-ocean boundary" is $\beta = 1.07 \pm 0.03$.

Crustal Thinning-Derived Stretching Factors

Crustal thinning-derived stretching factors for Palaeocene breakup are not presented since it is difficult to determine the relative thinning contributions from the earlier rift events in the Triassic, Jurassic, and Cretaceous. Furthermore, crustal thickening from Palaeocene igneous underplating adds additional controversy. For these reasons we do not present estimates of whole-crustal extension.

"Whole-Lithosphere" Stretching Factors

Palaeocene and late Upper Cretaceous lithosphere stretching has been derived from the flexural backstripping, decompaction, and reverse postbreakup subsi-

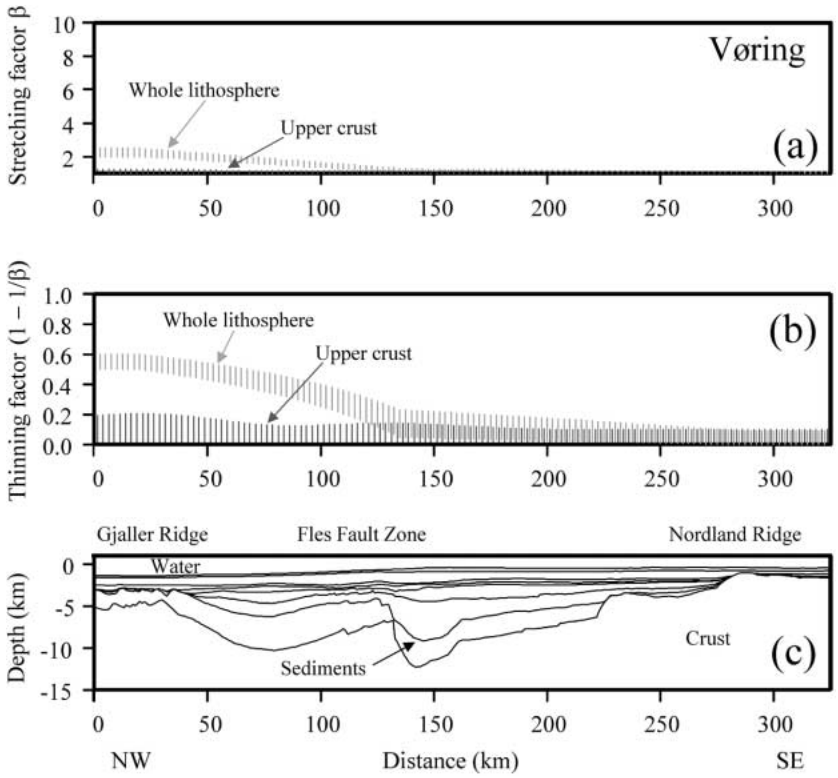

Figure 4.8 (a and b) Palaeocene stretching and thinning factors determined for upper crust and whole lithosphere for the Vøring rifted continental margin. (c) Upper-crustal section for the Vøring margin profile based on seismic data.

dence modeling of the stratigraphic section shown in figure 4.7c, which is derived from Dore et al. (1997). The assumption that the Base Tertiary unconformity at the Gjaller Ridge and Fles Fault Zones was at (or near) sea level in the Palaeocene has been used as the palaeobathymetric constraint for the flexural backstripping. While a range of values of T_e (0, 5, 10, and 25 km) were used in the flexural backstripping, these results are relatively insensitive to the value of T_e used, because the wavelength associated with loading is long. The resulting β-stretching-factor profile for the Palaeocene lithosphere-stretching event is shown in figure 4.8a and b assuming $T_e = 3$ km. The Palaeocene lithosphere-stretching factor, assuming no earlier late Jurassic-early Cretaceous rifting and no dynamic uplift from the Iceland plume, shows a value of 2.5 in the west of the profile decreasing toward 1 in the east.

Along the Norwegian margin, the determination of lithosphere-extension estimates derived from postbreakup subsidence history is complicated for the following reasons:

(a) Earlier late Jurassic-early Cretaceous and Triassic intracontinental rifting

The Norwegian margin has suffered a protracted rift history with large and distinct intracontinental rifting events occurring in the late Jurassic-early Cretaceous and Triassic prior to the formation of the rifted margin in the early Tertiary. Estimates of the magnitude of Palaeocene lithosphere stretching associated with continental breakup determined by flexural backstripping, decompaction, and reverse postbreakup subsidence modeling are sensitive to residual thermal subsidence from these earlier rift events. We therefore present results assuming likely bounding ranges on the timing and magnitude of earlier rift events.

Sensitivity of the determined magnitude of Palaeocene lithosphere stretching to earlier rift events is summarized in figure 4.9a and b. The effects of a large early Cretaceous rift event at 128 Ma (representing the end of late Jurassic-early Cretaceous rifting) with β stretching factors of 1.5 and 2 are examined. Inclusion of an earlier late Jurassic-early Cretaceous rift event reduces the magnitude of Palaeocene lithosphere stretching from $\beta = 2.5$ to 2.2 in the west of the profile for the preferred upper bound of $\beta = 1.5$ for the earlier late Jurassic-early Cretaceous rift event (Roberts et al. 1997).

(b) Igneous underplating

Igneous underplating generates permanent uplift providing that the density of the new material is less than the density of the asthenospheric mantle (Brodie and

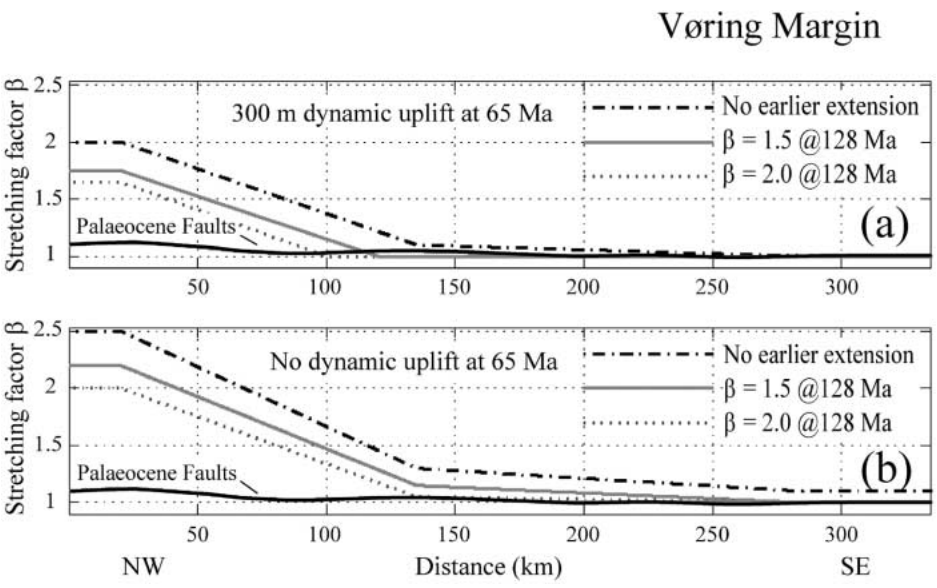

Figure 4.9 (a and b) Palaeocene stretching factors for whole-lithosphere extension of the Vøring rifted continental margin, determined by flexural backstripping and reverse postbreakup modeling, showing sensitivity to Palaeocene transient uplift from the Iceland plume and earlier Upper Jurassic-Lower Cretaceous rifting. Upper-crustal extension is significantly lower than "whole-lithosphere" extension under all reasonable circumstances of earlier rift event and transient plume uplift.

S
N
L

White 1995). The uplift magnitude may be estimated from the thickness of igneous underplating (inferred from wide-angle seismology) if the underplating density is known. In our analysis, we deliberately make the simplifying assumption that subsidence is assumed to result purely from cooling of the lithosphere. Therefore igneous underplating that predates the age of the palaeobathymetric marker probably makes little difference to the estimate of extension, whereas igneous underplating that postdates the palaeobathymetric marker buffers the predicted subsidence (by generating relative uplift) and reduces the estimated stretching factor. White and Lovell (1997) suggest that much of the emplacement of basaltic underplating in the North Sea occurs between 63 and 54 Ma. If, as it seems likely, significant underplating has occurred post 65 Ma (or in some cases post 57 Ma), then our "whole-lithosphere" stretching factors and extension discrepancies are underestimates. Simple calculations assuming Airy isostasy imply that a 5-km-thick underplated body distributed at any depth within the lithosphere generates 400–800 m of initial permanent uplift. Subsidence curves suggest that for an apparent stretching factor $\beta \sim 2$, the true stretching factor after correction for (say) $\sim$500 m of water-loaded uplift might increase by $\Delta\beta < 0.5$.

(c) Transient uplift from the Iceland mantle plume

Many basins in the northeast Atlantic experienced regional Palaeocene uplift and accelerated Eocene subsidence. Although several authors proposed that the accelerated Eocene subsidence is generated by a Tertiary stretching event (Joy 1992; Hall and White 1994), a consensus has emerged that the Eocene subsidence anomaly is generated by the decay of Palaeocene regional uplift event associated with the initiation of the Iceland plume (Bertram and Milton 1989; Nadin and Kusznir 1995). Regional plume-related dynamic uplift was probably close to zero at 65 Ma and reached a peak around $\sim$57 Ma (Nadin et al. 1997). Transient regional uplift due to a mantle plume at the time that the palaeobathymetric markers are to be restored must be considered when estimating the lithosphere-stretching factor using flexural backstripping and reverse postbreakup modeling. Nadin et al. (1997) presented evidence to show that the regional dynamic uplift associated with the initiation of the Iceland plume had a magnitude of the order of 300–500 m in the northern North Sea increasing to 900 m in the Faroe-Shetland Basin, and commenced in the mid-Palaeocene and rapidly decayed in the early Eocene. White and Lovell (1997) suggest that much of the emplacement of basaltic underplating in the North Sea occurred between 63 and 54 Ma, and is presumably synchronous with transient plume-related uplift.

Sensitivity of the determined magnitude of Palaeocene lithosphere to transient Palaeocene dynamic uplift associated with the initiation of the Iceland plume is shown in figure 4.9a and b. A magnitude of 300 m for transient plume uplift is assumed by comparing the distances of the North Sea observations (Nadin et al. 1997) and the Vøring Basin from the location of the initiating plume along the early Tertiary Faroes-Iceland-East Greenland aseismic ridge. The effect of including 300 m of Palaeocene dynamic plume uplift in the analysis is to decrease the

S
N
L

magnitude of the Palaeocene lithosphere stretching to $\beta = 2$ for the model with no earlier extension and to $\beta = 1.75$ when the earlier Upper Jurassic-Lower Cretaceous rift is included. The preferred estimate of Palaeocene lithosphere stretching by flexural backstripping assumes no transient plume uplift (figures 4.8a and b, 4.9b), because there is no evidence to suggest that the North Atlantic was dynamically supported by the early Iceland plume at 65 Ma.

Stretching Factor Variation with Depth on the Vøring Margin

For the Vøring margin, the preferred subsidence-derived estimate of the Palaeocene stretching event is $\beta = 1.6 \pm 0.2$; the stretching factor from seismically observable faulting in the Palaeocene section is $\beta = 1.07 \pm 0.03$. The profiles of Palaeocene stretching and thinning factors for the upper crust and for the whole lithosphere for the Vøring margin are shown in figure 4.8a and b. The corresponding stratigraphic cross section is shown in figure 4.8c. The preferred lithosphere-stretching factor profile assumes no dynamic plume uplift at 65 Ma and an earlier Upper Jurassic-Lower Cretaceous rift of magnitude $\beta = 1.5$. Stretching and thinning factors (figure 4.8a and b) for the lithosphere are significantly greater than those for the upper crust on the oceanward (west) side of the profile. These results are similar to and consistent with those of Roberts et al. (1997) who performed a similar analysis. Crustal thinning-derived extension estimates are not included because the partitioning of the observed present-day stretching factor between earlier rift events and/or igneous underplating is uncertain. Depth-dependent stretching appears to be present within ~100 km of the continent-ocean boundary for all reasonable assumptions of the magnitude of dynamic topography present at 65 Ma and the magnitude of the early Cretaceous rift event. The possibility of significant extension generated by dyke intrusion is discussed later in this chapter.

Stretching Observations on the South China Sea Rifted Margin (Pearl River Mouth Basin)

The South China Sea (figure 4.10a) is floored by oceanic crust, is surrounded by stretched continental crust, and has a Tertiary extensional origin. In the east, the oceanic crust of the South China Sea is subducting eastward and obliquely at the Manila Trench beneath the Luzon Arc (Pautot and Rangin 1989). This study focuses on the section of the northern continental margin of the South China Sea adjacent to the Pearl River Mouth Basin (also called the Zhujiangkou Basin) offshore of South China. The Pearl River Mouth Basin is 300 km wide, 800 km long, and trends northeast-southwest. The basin comprises a series of fault-bounded grabens and is filled with up to ~10 km of sediments (Lee and Lawver 1994). Regionally, the Pearl River Mouth Basin forms part of a chain of Tertiary basins in the Pacific Northwest that extend from Vietnam in the southwest to the Kuril

S
N
L

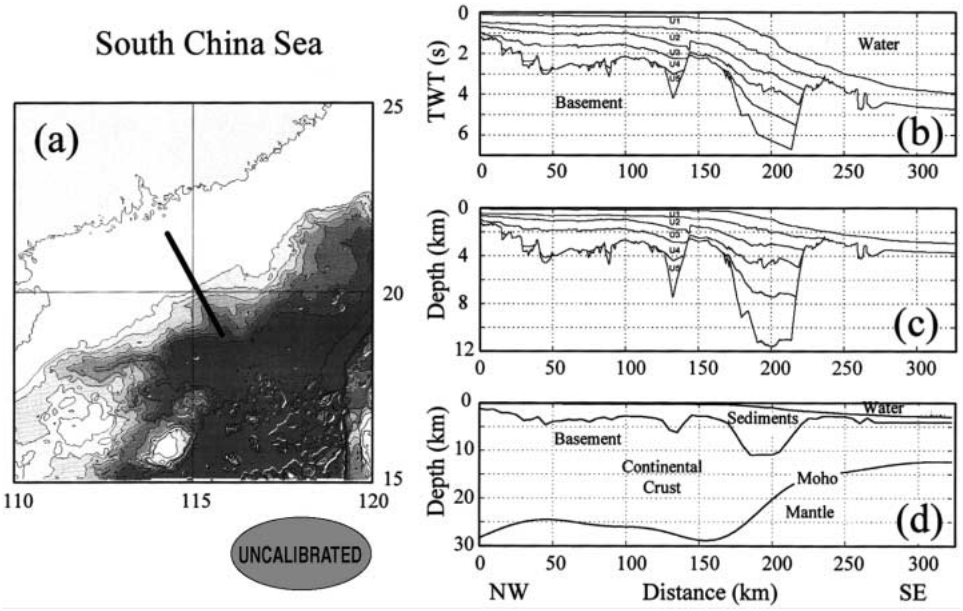

Figure 4.10 (a) Location map showing bathymetry of the South China Sea and the location of the Pearl River Basin profile used in this study. (b and c) Time- and depth-converted upper-crustal sections for the Pearl River Basin. Base U1 corresponds to base late Miocene; U2 and U3 Mid Miocene; U4 mid Palaeogene; U5 top basement (Turonian). (d) Crustal section based on seismic data and gravity data.

Basin, eastern Russia in the northeast. The spreading history of oceanic crust in the South China Sea is well known. East-west trending magnetic lineations correlate with magnetic anomalies 11–5D (32–17 Ma; Taylor and Hayes 1980, 1983; Briais et al. 1993) in the northwest subbasin and are in agreement with ages determined from a comparison of the heat-flow anomalies and plate-model predictions (Parsons and Sclater 1977; Lee and Lawver 1994). The South China Sea ocean basin is somewhat V-shaped (thinner in the southeast), where magnetic anomalies indicate that seafloor spreading began later (24–15 Ma; Briais et al. 1993). Seafloor spreading terminated with the emplacement of basaltic seamounts and other igneous bodies with ages 10–15 Ma.

Lithospheric extension in the Pearl River Mouth Basin occurred during the Palaeocene-Oligocene, although there is considerable uncertainty over the rifting history (Ru and Pigott 1986; Su et al. 1989). Ru and Pigott (1986) suggested that the Pearl River Mouth Basin has undergone at least three distinct tectonically pulsed rifting phases (late Cretaceous-Palaeocene, late Eocene-early Oligocene, and middle Miocene) with two intervening stages of seafloor spreading, whereas Su et al. (1989) suggest that the subsidence is consistent with a prolonged stretching event ($\beta \sim 1.8$) from the late Cretaceous to late Oligocene with a minor event in the Miocene ($\beta \sim 1.1$). However, in recent times age-dating of the stratigraphy

has been debated with new interpretations favoring systematic shifts to younger ages (Edwards 1992). In contrast, the spreading history of oceanic crust in the South China Sea is well constrained by magnetic anomalies.

The data used in this study are largely provided by BP and are summarized in figure 4.10b–d. Sedimentation rates in the Pearl River Mouth Basin appear to have maintained pace with subsidence, and the palaeobathymetries at all times are small. Su et al. (1989) report that the foraminifera, pollen, and spore assemblages from ~40 offshore wells indicate that the maximum palaeowater depths were <200 m and are significantly less than this from the post middle Miocene. Since few wells penetrate the syn rift, interval velocities for depth conversion (figure 4.10c) are taken from a BP-Amoco report (Moorcraft and Roberts 1991). Top basement in figure 4.10b–d corresponds to intra Upper Cretaceous (Turonian) age.

Upper-Crustal Stretching Factors

Upper-crustal extension was estimated by summing heaves on seismically resolvable faults offsetting top basement (figure 4.10b and c). A total of 33 seismically mappable faults were used to derive the upper-crustal stretching and thinning factor profiles shown in figure 4.11a and b. Fault-derived extension is 55 ± 10 km, which corresponds to a mean stretching factor $\beta = 1.3 \pm 0.05$. This result is consistent with Westaway (1994), but the stretching factor is significantly less than in the analysis of an interpretation of similar data by Su et al. (1989).

Crustal Thinning Stretching Factors

The depth to Moho is derived from an inversion of Bouguer gravity anomaly data that simultaneously solves for the residual thermal contribution from recent lithosphere stretching (Davis 1999) and is calibrated by wide-angle seismic estimates of Moho depth obtained by a nearby expanding spread profile (ESP) experiment (Nissen et al. 1995). The resulting crustal cross section is shown in figures 4.10d and 4.11c. Stretching and thinning factors determined from crustal basement thickness are shown in figure 4.11a and b. The total extension determined from crustal thinning from unstretched continental crust to the "continent-ocean boundary" is 140 ± 25 km (mean $\beta \sim 2.4 \pm 0.2$). and is consistent with the extension determined from the pseudo two-dimensional profile derived from ESP data (Nissen et al. 1995).

"Whole-Lithosphere" Stretching Factors

Given the substantial uncertainty in the ages of the mapped stratigraphic horizons and in the age of rifting, "whole-lithosphere" stretching factors from the Pearl River Mouth Basin are not reliable and are not presented.

S
N
L

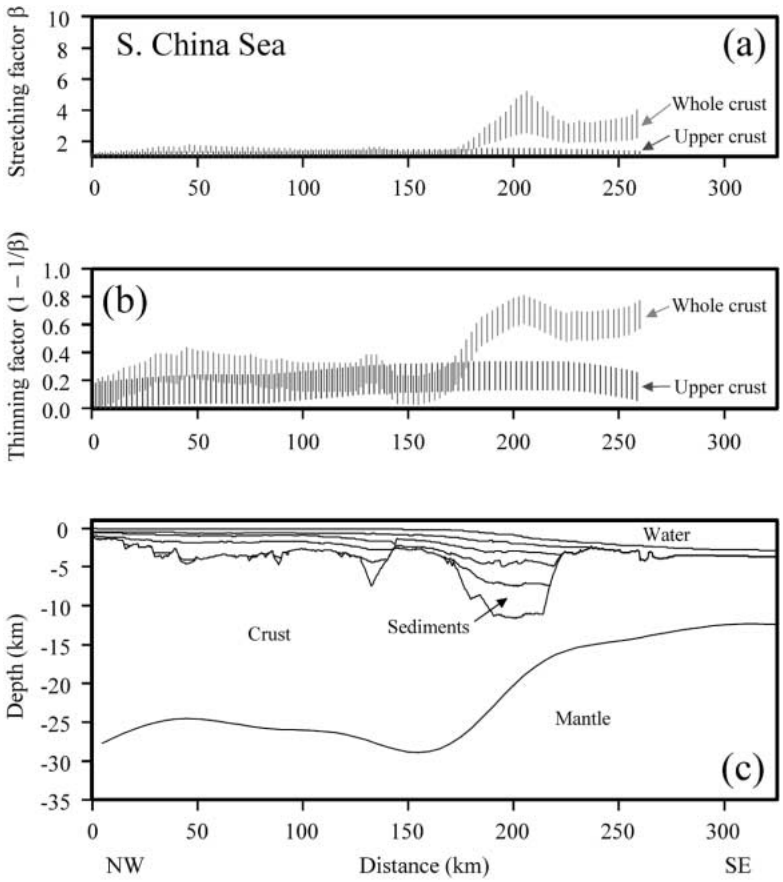

Figure 4.11 (a and b) Stretching and thinning factors determined for upper crust and whole crust for the South China Sea rifted continental margin (Pearl River Mouth Basin). (c) Crustal section for the Pearl River Basin margin based on seismic and gravity data.

Stretching Factor Variation with Depth on the South China Sea Margin

Stretching and thinning estimates derived from upper-crustal faulting and crustal thinning are compared in figure 4.11a and b for the Pearl River Mouth Basin segment of the South China Sea margin. Thinning estimates for the upper crust and whole crust are consistent in the northern part of the profile adjacent to mainland China, but as the continent-ocean boundary is approached southward whole crustal thinning greatly exceeds that for the upper crust and depth-dependent stretching becomes pronounced.

The interpretation of depth-dependent stretching in the Pearl River Mouth Basin is consistent with Westaway (1994) but contrary to that of Su et al. (1989). Su et al. (1989) derived stretching factors from faults, crustal thinning, and postrift thermal subsidence and suggested that there is no evidence for a significant extension discrepancy and that the main stretching event occurred during the late

Cretaceous-late Oligocene (ending at ~35 Ma) with β ~1.8. Although the consistency of the analysis of Su et al. (1989) seems impressive, Westaway (1994) used the same data to argue that extension factors demonstrate depth dependency with upper-crustal stretching factor β ~1.3. An advantage of this study of the Pearl River Mouth Basin is that the primary seismic data were used and depth conversion was performed with a well constrained velocity-depth function. Significantly more faults have been identified in the primary data. (Thirty-three faults are used in this study versus ten in Su et al. [1989]).

Observations of Depth-Dependent Stretching at Rifted Continental Margins: Reality or Artifact?

Independent methods and data sets have been used to determine upper-crustal, whole-crustal, and whole-lithospheric stretching factors for the Goban Spur, Galicia Bank, Vøring, and South China Sea continental margins; and the resulting profiles of stretching and thinning factor are summarized in figures 4.3, 4.6, 4.9, and 4.11. The total extension for each profile may be determined by integrating the thinning factor with respect to horizontal distance (equation 4.3). Total extension for each of the Goban Spur, Galicia Bank, Vøring, and South China Sea continental margins profiles are shown in figure 4.12 for upper crust and either whole crust or whole lithosphere. Upper-crustal and whole-lithosphere extension

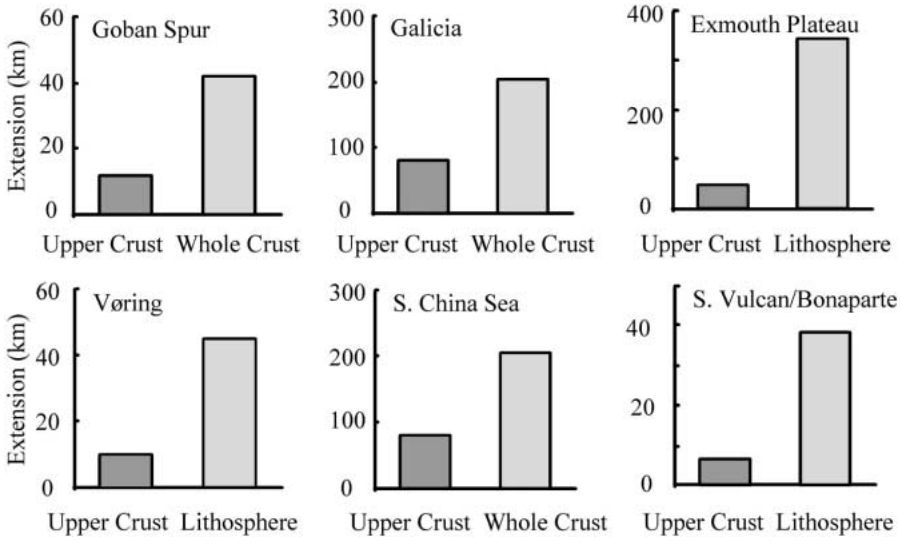

Figure 4.12 Summary of extension estimates at different depths within the lithosphere for Goban Spur, Galicia, Vøring, and the South China Sea (this study) and for the Exmouth Plateau (Driscoll and Karner 1998) and South Vulcan (Bonaparte) Basin (Baxter et al. 1999). In the Vøring margin, the estimates refer to the Palaeocene rifting event only.

estimates have also been determined for the northeast Australian rifted continental margin for the Exmouth Plateau, from stretching profiles published in Driscoll and Karner (1998), and the South Vulcan (Bonaparte) Basin from stretching profiles published in Baxter et al. (1999). In the Exmouth Plateau margin, the horizontal integration of thinning factor has been conducted from the continental edge of the transition zone at $x = -75$ km (Driscoll and Karner 1998) toward the continent to be consistent with the other extension estimates of figure 4.12.

In all of the rifted continental-margin examples shown in figure 4.12, the summed extension observed in the upper crust is substantially less than that observed for the whole crust or whole lithosphere. All cases studied show depth-dependent stretching of the continental lithosphere, where extension appears to increase with depth, over a width of 50–200 km adjacent to the continent-ocean transition. Whole-crustal and "whole-lithosphere" extension is typically a factor of ~3 larger than upper-crustal extension. Possible explanations, the majority of which we reject, are discussed in the next section.

Random Errors

Errors have been formally calculated for the thinning and stretching factors from upper-crustal faulting and whole-crustal thinning. As illustrated in figures 4.3, 4.6, 4.9, and 4.11, computed errors for thinning and stretching factors are significantly different (>1.5 standard deviations) within ~100 km of the "continent-ocean boundary" and converge toward the continent. The discrepancy between upper-crustal and whole-crust or whole-lithosphere stretching is therefore interpreted as being statistically significant.

Subseismic Resolution Faulting

Some of the extension by faulting of the upper crust is associated with small faults for which displacements are beneath the resolution of seismic reflection imaging. As a consequence, some upper-crustal extension by faulting will not be detectable using seismic reflection imaging techniques. Fault-scaling relationships enable quantification of subseismic extension and suggest that, for seismic reflection data, predicted missing extension amounts to ~35% of the observed extension (Walsh et al. 1991). Indeed, several authors have demonstrated that when subseismic extension is accounted for in intracontinental rift basins, independent estimates of extension based on thermal subsidence and faulting become comparable (Roberts et al. 1993; Marrett and Allmendinger 1992). Figure 4.13 illustrates the corrected (real) stretching factor (β_r) as a function of the observed (apparent) stretching factor (β_a) where f is defined as one plus the missing extension fraction.

$$\beta_r = \frac{\beta_a}{\beta_a + f(1 - \beta_a)} \tag{4.7}$$

S
N
L

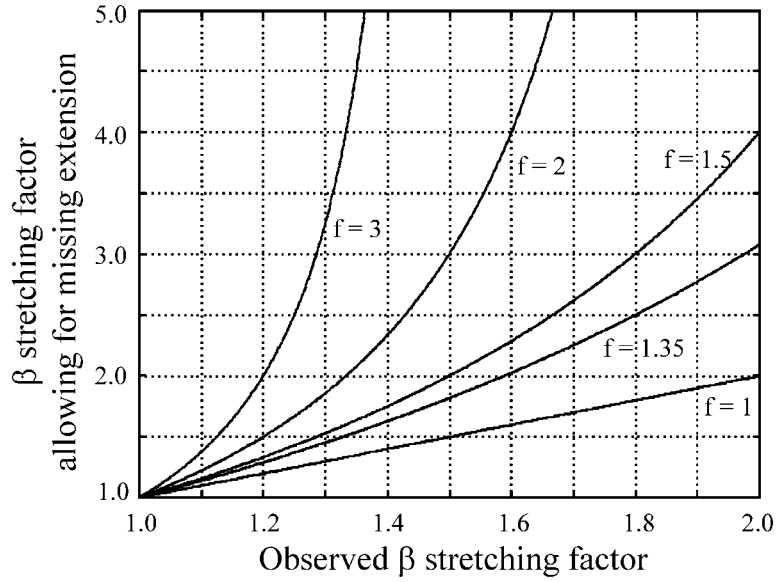

Figure 4.13 "True" (i.e., corrected) stretching factor against apparent (observed) stretching factor as a function of the missing extension factor f as described in the text.

For $f = 1.35$ (35% missing extension; Walsh et al. 1991), faulting beneath the resolution of seismic reflection imaging cannot explain the large extension discrepancies at rifted margins. Explanation of our observations using this principle alone requires unreasonable missing extension fractions and seems unlikely.

Fault Geometry

In this chapter, the calculation of upper-crustal extension assumes that upper-crustal faults have a planar geometry. The use of a listric geometry, however, makes little difference in practice to extension estimates, because the fault angle changes little with depth in the upper part of the seismic reflection sections where fault offsets are measured. Studies of actively extending regions in continents (Turkey, Greece, and western United States) suggest that active basement faults are planar to at least depths of 10 km (Jackson and McKenzie 1988; Jackson 1987; Stein and Barrientos 1985). Although basement faults may appear to be listric on time sections, several authors have demonstrated that typical basement faults are planar in depth (Kusznir and Ziegler 1992) as confirmed by prestack depth migration on the outer Galicia (Reston 1996).

Second-Generation Faults

If extension of the lithosphere at rifted margins is associated with multiple generations of faults that cut earlier generations and mask their detection, our method

of estimating upper-crustal extension underestimates upper-crustal extension. Stretching of the upper crust has been determined using seismic reflection data, which allows good imaging of the syn- and prebreakup stratigraphy required to determine fault-controlled extension. In the Goban Spur, Galicia Bank, and the outer parts of the Exmouth Plateau and Pearl River Basin, these margins are sediment starved with little postbreakup deposition obscuring deeper stratigraphy. No second-generation faulting has been observed on the seismic data used in this study. Whilst contributions from second-generation faulting cannot be ruled out, it is notable that the fault-derived stretching factor profiles at rifted margins are relatively constant, with typical maximum stretching factors around $\beta \sim 1.3$, and are considerably less than those observed in many intracontinental rift basins where second-generation faulting is not believed to occur (Roberts et al. 1993).

Nonbrittle (Aseismic) Extension

Upper-crustal extension could be underestimated if upper-crustal extension occurred aseismically rather than by faulting. Upper-crustal extension might conceivably occur through dyking or nonbrittle (plastic) deformation. While dyking is possible, it is difficult to see how it may occur up to ~100 km from the continent-ocean boundary. Furthermore, at nonvolcanic rifted margins the transitional region between rotated continental fault blocks in thinned continental crust and unequivocal oceanic crust is surprisingly devoid of significant basaltic volcanism. margins (e.g., Iberian Margin; Whitmarsh et al. 2001). Present-day analogues suggest that the majority of upper-crustal deformation is accommodated by seismic slip on faults (Jackson 1987). Studies of the actively extending Aegean region place good constraints on both geodetic and upper-crustal fault-related strain. That the seismically determined velocity field in the Aegean is comparable with the estimate predicted from simple kinematic arguments (i.e., plate-motion studies) suggests that the majority of the deformation in the upper crust is accommodated by seismic slip on faults (Jackson and McKenzie 1983).

Intrusion of Dense Melt into the Lithosphere and Phase Transitions

Emplacement and cooling of ultramafic melts may thin the seismically defined crust, giving rise to errors in our determination of crustal thinning and stretching. However, the addition of crustal material generates uplift, not subsidence, unless underplating occurs in the eclogite stability field, which is unlikely (McKenzie 1984). The anomalously high postrift subsidence observed at the outer ~100 km of rifted continental margins is therefore not readily explained by melt intrusion. Phase transformation from gabbro to eclogite or garnet granulites would raise the Moho by thinning the crust, and load the lithosphere and generate subsidence, but is unlikely to occur at depths shallower than ~50 km.

Mantle Serpentinization

Serpentinization of mantle reduces both its seismic velocity and density such that it could apparently thicken the crust. Such a process would therefore serve to mask rather than enhance the observed increase in thinning and stretching with depth. While many rifted continental margins are associated with a transitional region consisting of serpentinized mantle between unequivocal continental and unequivocal oceanic crust (Pickup et al. 1996), this explanation cannot explain the observed discrepancy between whole-crustal and upper-crustal stretching factors.

Rifting above Sea Level

Rifting above sea level is likely to erode upper-crustal fault blocks, thereby destroying the fault record, leading to an underestimation of upper-crustal stretching from fault-heave measurements. Whereas the uniform lithosphere stretching model (McKenzie 1978) predicts uplift where the initial crustal thickness <18 km, isostatically compensated lithosphere with thin crust should be associated with significant prerift bathymetry, which buffers the subsequent uplift. Alternatively, rifting might occur above sea level if the lithosphere suffers depth-dependent stretching. Analytical models of two-layer stretching demonstrate that uplift is only predicted if the mantle-thinning factor (ε) is greater than 2.2 times the crustal thinning factor (Royden and Keen 1980) and that subsidence is always generated (regardless of mantle-stretching factor) provided that the stretching factor $\beta > 1.5$. While some erosion of fault block crests is observed on all four rifted margin profiles presented in this chapter, the amount of upper-crustal extension "lost" through fault-block crest erosion is believed to be small.

Influence of a Mantle Plume on Subsidence

Anomalous subsidence patterns on rifted margins may sometimes be attributable to mantle-plume influences (Nadin et al. 1997). Whereas plume collapse-driven subsidence may occur simultaneously with post-rift thermal subsidence (e.g., the Norwegian margin), it alone cannot account for the observed subsidence anomaly (see also Roberts et al. 1997). Depth-dependent stretching is also observed at "nonvolcanic" margins that are not associated with mantle-plume activity (e.g., Galicia, Goban Spur).

Flexural Coupling

Unstretched continental crust that is strongly coupled mechanically to adjacent thermally subsiding oceanic lithosphere is expected to experience postbreak subsidence greater than that predicted from its own thinning and stretching. Provision has been made on our analysis to account for the enhanced subsidence of conti-

S
N
L

nental crust adjacent to oceanic crust in the reverse postrift modeling analysis by requiring the stretching factor to ramp to $\beta = \infty$ at the conventional continent-ocean boundary. Sensitivity analysis to T_e used to define this coupling has also been performed. Anomalously large lithosphere-stretching estimates for the continental margin lithosphere from subsidence backstripping due to flexural coupling to oceanic lithosphere is therefore ruled out.

Lithosphere Extension on a Low-Angle Extensional Detachment (Simple Shear)

All rifted margins studied in this chapter show greater thinning and stretching of the whole crust and lithosphere than that observed for the upper crust, consistent with similar reports at other margins (Driscoll and Karner 1998). Driscoll and Karner (1998) have noted that all margins appear to be derived from the "upper plate" of a possible simple-shear model (Wernicke 1985; Lister et al. 1991), giving rise to the "upper-plate paradox." The "upper-plate paradox" and simple-shear models of lithosphere extension are discussed further in Discussion and Summary. Although instances of active low-angle faults accommodating lithosphere extension (Wernicke 1985) have been reported (Abers 1991), their existence has been disputed. Jackson and McKenzie (1983) note that there is "not one single example of seismic activity on a subhorizontal fault [dip $<20°$]"; indeed, the vast majority of seismically active normal faults have dips in from 30–60°. Therefore, if active low-angle normal faults exist, they must occur beneath the earthquake nucleation depth. Although several authors claim to have imaged a detachment either in the field or on seismic reflection profiles (Torres et al. 1993), very little seismic evidence exists for their presence in extensional settings (Collier and Watts 1997). Probably the best example of a possible candidate for such a detachments is a the so-called S-reflector off Galicia (Reston 1996; Charpal et al. 1978).

Lower-Crustal Buoyancy-Driven Flow

Buoyancy-driven flow in the lower crust could give rise to enhanced apparent thinning and stretching of the continental crust at rifted margins. Lower-crustal flow appears not to occur during the formation of intracontinental rift basins since the uniform stretching model is consistent with equal extension observed in the upper crust, the whole crust, and lithosphere (McKenzie 1978; White 1990; Marsden et al. 1990; Roberts et al. 1993). Although thickening of thinned continental crust by buoyancy-driven lower-crustal flow has been proposed (Buck 1991; Davis and Kusznir 2002), if it were to exist it would serve to counteract rather than enhance the observation of crustal thinning and stretching increasing with depth. While lower-crustal flow may occur at rifted continental margins, it is unlikely to contribute to the total extension estimates presented in this paper

unless the lower-crust flows into the domain which is conventionally believed to be oceanic.

Model Predictions of Depth-Dependent Stretching at Rifted Margins

We use simple analytical solutions and two-dimensional finite-element models of the divergent lithosphere flow that is expected to occur during early seafloor spreading to explore the mechanism responsible for depth-dependent lithosphere stretching observed at rifted continental margins. The models aim to investigate the effects of early seafloor spreading on the newly formed continental margin lithosphere; they do not investigate the prebreakup rifting of continental lithosphere. The objectives are not to simulate the actual development of a rifted continental margin, but rather to investigate the physics of the conditions under which depth-dependent stretching may occur.

Analytical Solution for Corner Fluid Flow Applied to Young Seafloor Spreading

Insight into the origin of depth-dependent stretching observed at rifted continental margins may be derived from examination of the fluid-flow field at mid-ocean ridge spreading centers. The results for the analytical solution (Batchelor 1967) for corner flow for isoviscous incompressible mantle in which fluid upwells beneath a ridge before spreading laterally as the lithospheric plates diverge is illustrated in figure 4.14. While the two-dimensional corner-flow model for constant viscosity shown in figure 4.14 is highly simplistic, fluid-flow fields predicted by complex models that incorporate temperature-dependent viscosity and melt generation (Spiegelman and McKenzie 1987; Cordery and Phipps-Morgan 1992; Spiegelman and Reynolds 1999) are not dissimilar. The divergent velocity field has been computed for horizontal surface and vertical ridge axis velocities of 5 cm/yr; flow vectors are plotted normalized to this boundary condition.

In the reference frame of the ocean ridge we see a divergent horizontal flow balanced by upwelling beneath the ridge axis (figure 4.14). Only one half of the flow field is plotted because the flow field is symmetric about the ocean ridge axis. The same flow field may be transformed into the reference frame of the adjacent ocean basin or continental interior by subtracting the far-field ocean basin velocity vector. This flow field referenced to the ocean basin is shown in figure 4.14b. The depth dependency of the ocean ridge divergent flow field can be clearly seen in figure 4.14b. The flow field shows oceanward flow of the continental lithosphere mantle and lower crust of the adjacent newly formed rifted continental margin. Figure 14b demonstrates that the divergent motion of the adjacent young seafloor spreading center drives depth-dependent stretching in young rifted continental margin lithosphere.

S
N
L

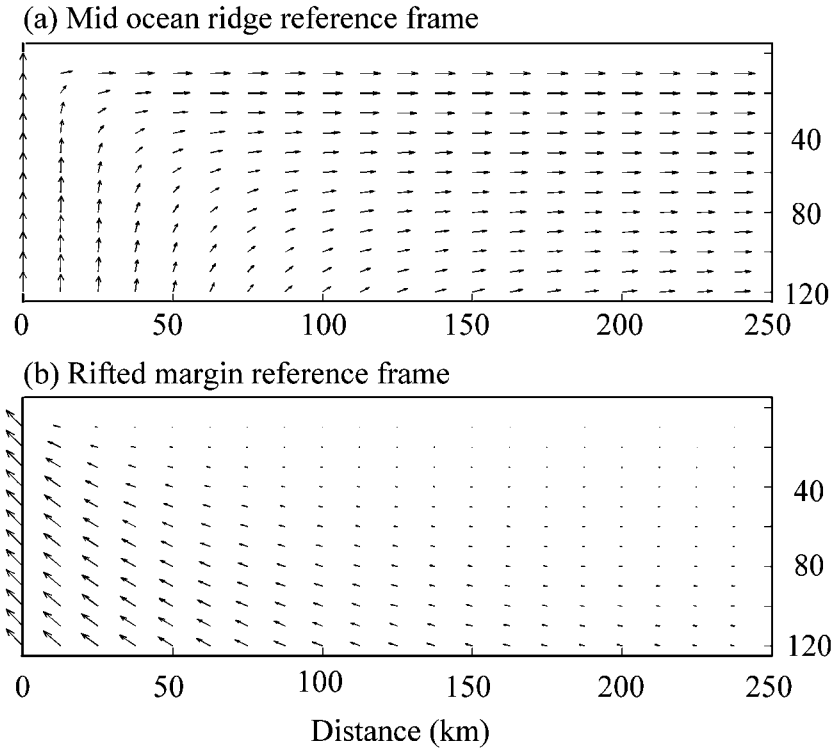

Figure 4.14 Fluid-flow velocity vectors for a simple two-dimensional analytical corner flow model of a mid-ocean ridge-spreading center using an isoviscous fluid: (a) in the reference frame of the mid-ocean ridge; and (b) in the reference frame of the far-field ocean basin or continental interior. Depth-dependent flow can be seen clearly in (b) where deeper material flows oceanward relative to upper lithospheric material.

Finite Element Modeling of Young Seafloor Spreading

The analytical corner-flow solution described above assumes constant viscosity, whereas the real viscosity structure associated with a young oceanic spreading center and adjacent continental-margin lithosphere is expected to be highly heterogeneous because of both temperature and compositional variations. While a full dynamic thermal and temperature-dependent viscosity solution is beyond the scope of this study, we have used finite-element modeling to examine depth-dependent stretching in an Earth model with a horizontally and vertically heterogeneous viscosity distribution. We emphasize that the aim of this simple finite element model is to investigate the effects of early seafloor spreading on the young rifted margin lithosphere and is not to investigate the effects of prebreakup intracontinental rifting that usually precedes continental breakup and the initiation of seafloor spreading.

The viscosity structure of this simple schematic model is shown in figure 4.15a. The finite-element model assumes that the cooler continental lithosphere has a greater viscosity than the hotter asthenosphere and that the continental lithosphere

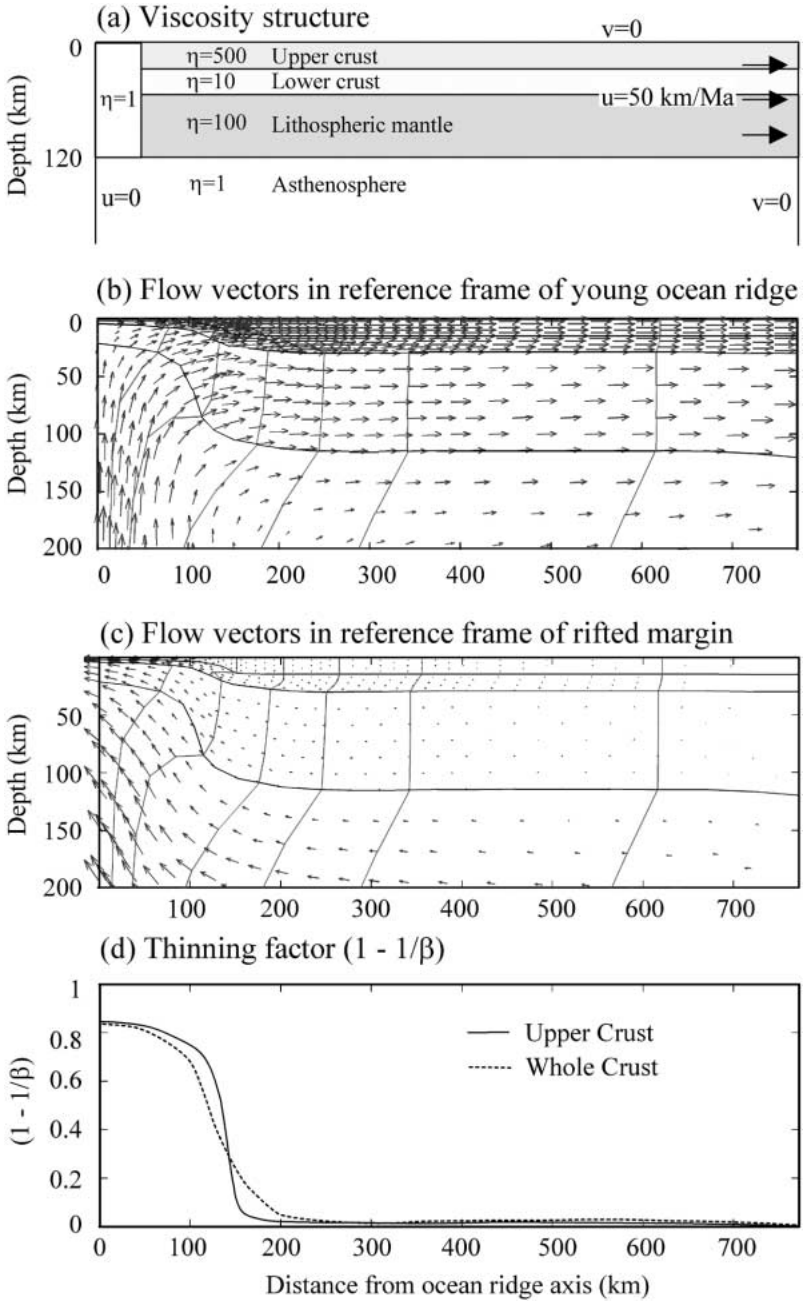

Figure 4.15 Simplified finite-element fluid-flow model of young seafloor spreading and adjacent rifted margin. (a) Viscosity structure and boundary conditions used in the finite-element model. Viscosities: upper crust $= 5 \times 10^{22}$ Pas; lower crust $= 1 \times 10^{21}$ Pas; lithospheric mantle $= 1 \times 10^{22}$ Pas; and asthenosphere $= 1 \times 10^{20}$ Pas; a vertically defined weak zone is present with viscosity $= 1 \times 10^{20}$ Pas. (b) Velocities predicted by the finite-element model in the reference frame of the young ocean ridge. (c) Velocities predicted by the finite-element model in the reference frame of the adjacent rifted margin. (d) Predicted thinning factors for the upper and whole crust.

S
N
L

is rheologically layered with a quartz-feldspathic crust above an olivine mantle (Kusznir and Park 1987). The young seafloor-spreading center is represented by a prescribed low-viscosity weak zone that is given the same viscosity as the asthensophere. The viscosity of the topmost mantle is assumed to be higher than that of the lower crust, because olivine rheology of the mantle is stronger than that of the quartz-feldspathic crust at the same temperature; and the viscosity of the lower crust is assumed to be lower than that of the upper crust because it is hotter (Kusznir and Park 1987; Kusznir 1991). The finite-element model is run with a constant-velocity far-field boundary condition of 50 km Ma^{-1} (5 cm/yr) for 2.5 Ma, and it is symmetric about an axis of symmetry at $x = 0$ km corresponding to the young seafloor-spreading axis. The top and bottom boundary conditions of the finite-element fluid model have zero vertical fluid velocity, and the model is 660 km deep corresponding to the base of the upper mantle.

The fluid-flow pattern predicted by the finite-element model in the reference frame of the young seafloor-spreading center is shown in figure 4.15b. The divergent motion of the flow field away from the spreading axis can be seen. The same flow field, transformed into the continental interior reference frame, is shown in figure 4.15c. This flow field shows oceanward flow of the mantle and lower crust of the continental margin lithosphere, similar to the analytical solution described in the previous section, and demonstrates that depth-dependent stretching occurs in the continental lithosphere adjacent to the young seafloor-spreading center.

Upper-crustal and whole-crustal thinning factors ($1 - 1/\beta$) predicted by the finite-element modeling are plotted in figure 4.15d. At distances greater than 150 km from the spreading axis in the postextension reference frame (corresponding to 40 km in the preextension reference frame), the stretching and thinning of the upper crust is predicted to be less than that of the whole crust with the discrepancy decreasing toward the continental interior. These predictions of the finite-element modeling are consistent with observations of thinning at rifted margins. Oceanward of 150 km (and in the region not covered by our observations of rifted margin thinning), the modeled stretching of the upper crust is predicted to exceed that of the whole crust. We identify that the form of predicted depth-dependent stretching is similar to that observed (and inferred) at rifted continental margins, provided that: (a) the lithosphere is horizontally rheologically layered with viscosity varying as a function of depth, and (b) the lithosphere possesses a vertically defined weak zone. In addition, a low-viscosity lower crust is required to generate depth-dependent stretching at the crustal level.

The viscosity structure of real oceanic and continental lithosphere at a young rifted margin is highly temperature- and time dependent due to conductive diffusion and advection of heat. A coupled transient thermal and fluid-flow model incorporating temperature-dependent viscosity and compositionally dependent rheology is required, but it is numerically difficult because of the large dynamic range of viscosity required and is beyond the scope of this chapter. However, preliminary models that incorporate conductive and advective contributions to the fluid-flow modeling of a temperature-dependent and compositionally varying rheology with a viscosity range of 10^{20}–5×10^{22} Pas (a factor of 250) have been

performed and show flow vectors and thinning profiles with depth-dependent stretching similar to that of figure 15. This exploratory model also suggests that depth-dependent stretching is small for small amounts of stretching but rapidly increases for $\beta > 2$ and may explain why intracontinental rift basins generally are consistent with the uniform stretching model (McKenzie 1978; Cordery and Phipps-Morgan 1992) and rifted margins are not.

Discussion and Summary

Area Conservation during Depth-Dependent Stretching

Depth-dependent stretching has been observed at a number of rifted continental margins, whereby stretching of the upper continental crust appears to be much less than that of the whole crust or lithosphere. Assuming that this observation is real, how is it possible for stretching to occur without violating area and hence volume conservation? To conserve volume, we require the upper-crustal, lower-crustal, and lithospheric mantle all to suffer the same total extension. In the stretched reference frame the horizontal integral of the thinning factor (ε) along the margin should be a constant:

$$E_{\text{tot}} = \int_0^\infty \varepsilon_{\text{uc}} \mathrm{d}x = \int_0^\infty \varepsilon_{\text{lc}} \mathrm{d}x = \int_0^\infty \varepsilon_{\text{ml}} \mathrm{d}x \tag{4.8}$$

The analytical and finite-element models described in the previous section obey the principle of volume conservation and also, under the conditions described, show depth-dependent stretching behavior (figures 4.14 and 4.15). The apparent extension discrepancy, generated where continental upper-crustal stretching factors are less than whole-crustal and lithosphere mantle-stretching factors, may be resolved by the presence of a region farther toward the ocean with an extension discrepancy of opposite polarity (figure 4.16a) so that the equality of the horizontal integral of extension with depth is maintained (equation 4.8). This would require that somewhere oceanward the upper continental crust is strongly stretched and thinned by an amount greater than deeper material. The existence of an oceanward region where upper crustal extension exceeds that of the whole crust and lithosphere is supported by the crossover of upper and lower lithosphere thinning factors predicted by the finite-element model and shown in figure 4.15d.

Evidence for Mantle Exhumation and a Transitional COB

Evidence for the exhumation of continental mantle at rifted continental margins is derived from drilling, dredging, seismic refraction, and wide-angle reflection

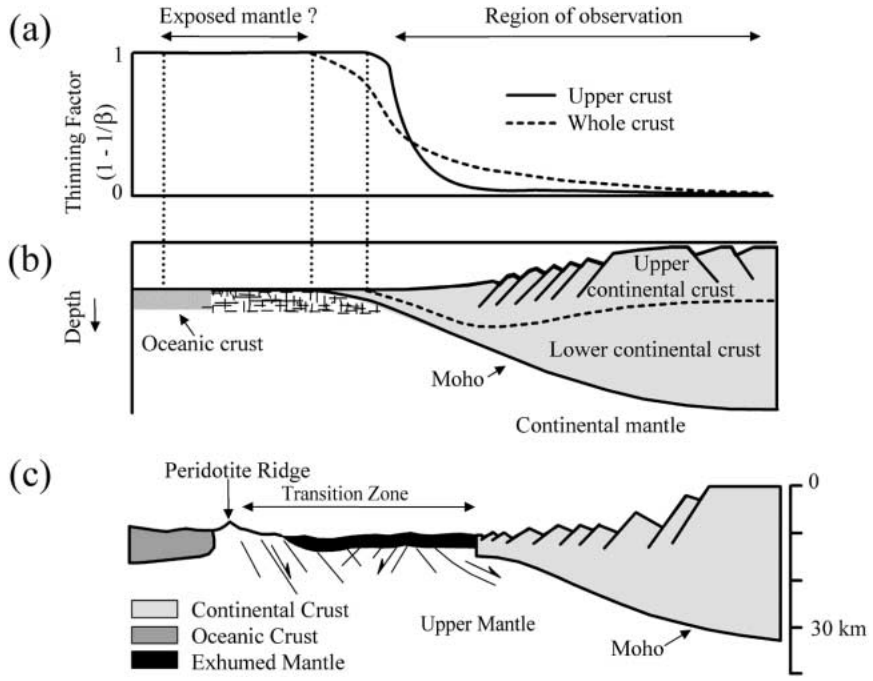

Figure 4.16 Conceptual diagram illustrating depth-dependent stretching and mantle exhumation at rifted continental margins. (a) Thinning factor for upper and whole crust illustrating depth-dependent stretching. In the region we observe, upper-crustal extension is less than that of the whole crust (and mantle); however, mass conservation requires upper-crustal extension oceanward to exceed that of the whole crust (and mantle). (b) Depth-dependent stretching and oceanward flow of continental mantle may lead to exhumation of continental mantle oceanward of thinned continental crust. (c) Schematic diagram of Iberian rifted margin structure showing mantle exhumation between oceanic crust and the rotated fault blocks of thinned continental crust, modified after Pickup et al. (1996).

surveys, normal-incidence seismic reflection, field analogs, and geochemistry (Pickup et al. 1996; Whitmarsh et al. 2001). In addition to field observations, mantle exhumation is also predicted by laboratory analogue models (Brun and Beslier 1996).

Evidence for Transitional Crust from Drilling and Dredging

Prominent ridges drilled in the region between unequivocal oceanic and unequivocal continental crust at the Iberian Abyssal Plain margin consist of highly serpentinized peridotite that appears to have undergone limited melt extraction and may represent exhumed continental mantle (Discovery 215 Working Group 1998; Whitmarsh et al: 2001). Whitmarsh et al. (2001) report that the exhumed mantle on the Iberian margin is "magma-poor" and contains relatively little basaltic material. This paucity of basaltic material within exhumed mantle may be consistent with mantle exhumation occurring during early seafloor spreading such that that

basaltic melt is focused (or sucked) into the ridge axis by the matrix pressure field associated with the divergent flow in the lithosphere and asthenosphere at the young ocean ridge (Spiegelman and McKenzie 1987; Spiegelman and Reynolds 1999).

Evidence from Seismic Refraction, Wide-Angle Reflection, and Normal Incidence Reflection

Seismic modeling of refraction and wide-angle reflection data from Galicia Bank reveals that the seismic Moho is frequently poorly defined in the "oceanic" domain adjacent to continental crust and that high-velocity (possibly serpentinitic) bodies are found at shallow depths (Pickup et al. 1996). Throughout the transitional zone, the seismic velocity is not typical of either oceanic or continental crust, because high velocities are found at shallow depths and normal mantle velocities are sometimes not detected. Although there are several possible alternative explanations for the seismic characteristics of the transition zone (ultraslow seafloor spreading, highly thinned and intruded continental crust, and unusually cool mantle), it is likely that the zone comprises continental upper mantle exhumed along a detachment zone and later serpentinized by seawater (Pickup et al. 1996)—a hypothesis consistent with the absence of true crust, and a reflection and refraction Moho. High-velocity zones are frequently noted to bound rifted margins and include the south Australia margin and the Tyrrhenian Sea (Decandia and Elter 1969) and may represent serpentinite belts, although the possibility remains that these zones may represent underplating where drilling has not occurred. Similar transition zones between unequivocal "oceanic" and "continental" crust have also been recognized at rifted continental margins including the Labrador Sea, Galicia, the Lincoln Sea, the Red Sea, and the Gulf of Guinea.

Field Analogs Provide Support for Mantle Exhumation Models

Preserved rift and seafloor-spreading structures in the Austroalpine and Penninic nappes of Graubünden, eastern Switzerland, provide evidence of detachment faulting and mantle exhumation. In particular, absence of normal components of oceanic crust (layers 2A and 2B, i.e., pillow lavas, sheet lava flows, and dykes) in some complexes have led several authors to propose that subcontinental mantle material was tectonically denuded and exposed at the seafloor during rifting (Manatschal and Nievergelt 1997; Manatschal and Bernoulli 1999). The similarities between the mode of extension inferred at both fossil and modern rifted margins provide support for the notion of depth-dependent stretching.

Additional Comments on Mantle Exhumation

Figure 4.16c shows the configuration of exhumed mantle at the Iberian continental margin proposed by Pickup et al. (1996). The exhumed mantle lies between the rotated fault blocks of the extensionally thinned continental crust and unequivocal oceanic crust out to the west. The existence of an oceanward region where upper-

crustal extension and thinning exceeds that of the lower crust and lithospheric mantle, as required by volume conservation (equation 4.8) and predicted by finite-element modeling (discussed under Area Conservation during Depth-Dependent Stretching), does not necessarily require the thinning of the upper crust to zero and the resulting exhumation of lower continental crust or continental mantle. However, the observation of exhumed continental mantle at rifted continental margins between the extensionally thinned continental crust and normal oceanic crust suggests that the continental crust may be thinned to zero thickness by the depth-dependent stretching process, allowing the continental mantle to be pulled out oceanward from under the continental crust and exhumed at the sea bed (figure 4.16b).

The "Upper-Plate Paradox"

Two end-member models of lithosphere extension have been proposed (figure 4.17a and b): the pure-shear-stretching model (McKenzie 1978), in which lithosphere stretching is uniform with depth, and the simple-shear model (Wernicke 1985), in which lithosphere extension is controlled by a low-angle lithosphere scale extensional detachment. For intracontinental extension and the formation of intracontinental rift basins, lithosphere extension is observed to be uniform with depth (White 1990; Roberts et al. 1993; Marsden et al. 1990) and the pure-shear (uniform) lithosphere extension model appears to apply (McKenzie 1978). Depth-dependent stretching as observed at rifted continental margins (Driscoll and Karner 1998; Roberts et al. 1997; Baxter et al. 1999; this study) is not consistent however with the "pure-shear" (uniform) lithosphere-extension model. Depth-dependent stretching is, however, predicted by the simple-shear lithosphere extensional detachment model.

The observations of depth-dependent stretching presented in this chapter for the Goban Spur, Galicia Bank, Vøring, and South China Sea margins show that stretching increases with depth, which is consistent with an " upper-plate" location for these margins in the context of the simple-shear lithosphere extensional detachment model (Wernicke 1985). This supports the observation of Driscoll and Karner (1998) that all rifted continental margins correspond to the "upper plate" of a lithosphere " simple-shear" extension model. Driscoll and Karner (1998) note that " upper-plate" scenarios have been proposed for both the Newfoundland and Galicia continental margins (figure 17c and d) yet these margins are conjugate to each other so that they cannot both be "upper plate" within the context of a simple-shear lithosphere extensional detachment model. Driscoll and Karner (1998) name this the "upper-plate paradox."

A possible explanation of the "upper-plate paradox" consistent with depth-dependent stretching and mantle exhumation at rifted continental margins is presented in figure 4.18. If depth-dependent stretching and mantle exhumation are generated by the early seafloor-spreading process, then depth-dependent stretching and mantle exhumation should occur simultaneously and symmetrically on both conjugate margins. Depth-dependent stretching is probably achieved by decou-

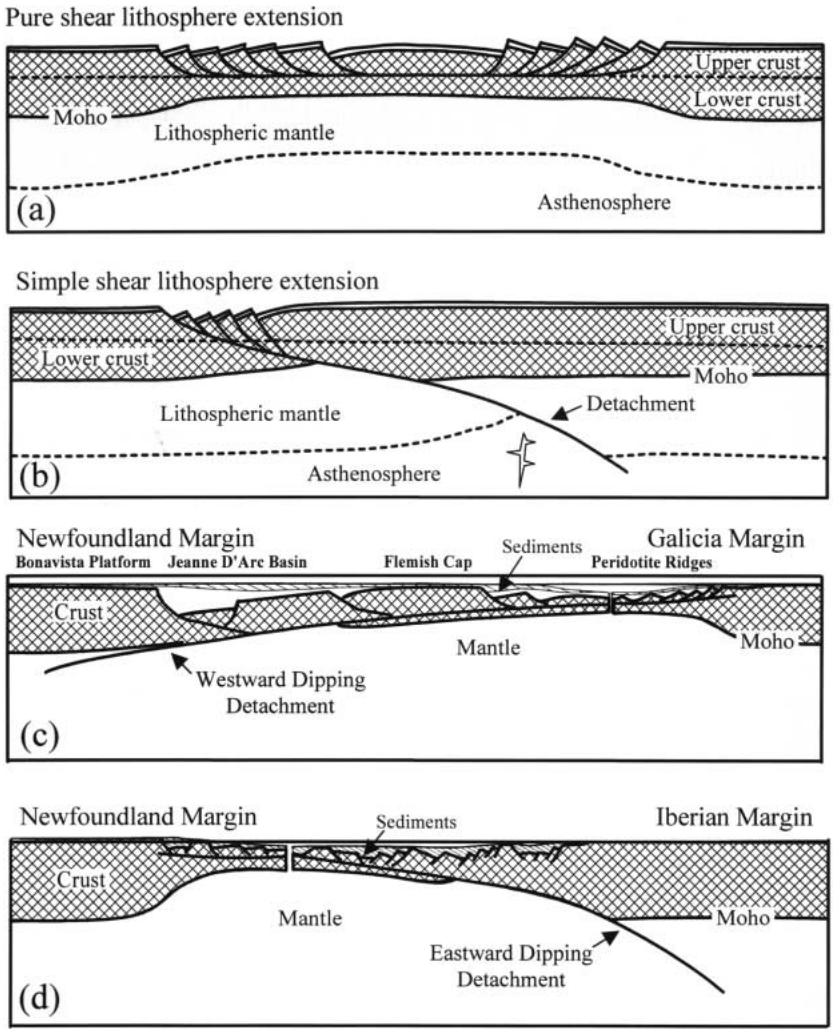

Figure 4.17 (a) Pure-shear (uniform) lithosphere-stretching model (McKenzie 1978) and (b) simple-shear lithosphere-stretching model (Wernicke 1985), adapted from Lister et al. (1986). The observation of increasing stretching with depth at rifted continental margins (Driscoll and Karner 1998; Roberts et al. 1997; Baxter et al. 1999; this study) is consistent with an "upper-plate" location (in the context of simple-shear lithosphere-stretching model; Wernicke 1985) for rifted margins. Driscoll and Karner (1998) named this the "upper-plate paradox." (c and d) Inconsistent interpretations of the form of lithosphere stretching at the Newfoundland and Galicia rifted continental margins identified by Driscoll and Karner (1998); (c) shows a westward-dipping lithosphere extensional detachment, while (d) shows an eastward-dipping lithosphere extensional detachment. Both "upper-plate" and "lower-plate" scenarios have been proposed for the Newfoundland and Galicia margins. If the Newfoundland and Galicia margins are conjugate margins, then the interpretations shown in (c) and (d) are inconsistent.

S
N
L

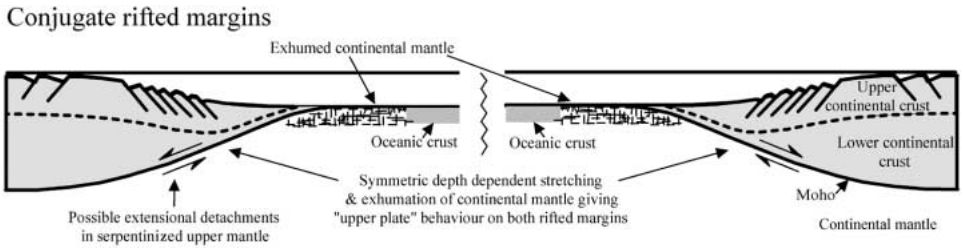

Figure 4.18 Conceptual diagram showing symmetric depth-dependent stretching and exhumation of continental mantle on conjugate rifted margins. The "upper-plate paradox," whereby all rifted continental margins appear to correspond to the hanging-wall of a lithosphere scale extensional detachment, may be explained by depth-dependent stretching and mantle exhumation on both conjugate margins as illustrated.

pling of the upper and lower crust from the continental mantle, either at discrete shear zones or more likely, since detachments are rarely observed, diffuse detachment zones. The conjugate margins would therefore be symmetrical with either discrete or diffuse detachment zones dipping downward toward the continent (figure 4.18), and consequently, both conjugate margins would suffer depth-dependent stretching consistent with the "upper plate" of a lithosphere simple-shear extensional detachment model. The timing of depth-dependent stretching and mantle exhumation with respect to the onset of seafloor spreading is however unknown and unconstrained at present. We suggest that the determination of the timing of depth-dependent stretching with respect to the onset of seafloor spreading is an important priority for future work.

Acknowledgments

We thank Mike Cheadle, Neal Driscoll, Garry Karner, Eric Lundin, Tim Minshull, Alan Roberts, Nicky White, and Bob Whitmarsh for helpful and stimulating discussions. Eric Lundin (Statoil) and Dave Roberts (BP) are thanked for providing seismic data. We also thank Uri ten Brink, Olaf Svenningsen, Neal Driscoll, and David Kohlstedt for constructive reviews. This work was conducted with support to MJD from a NERC Ph.D. studentship GT4/95/165/E.

References

Abers, G. 1991. Possible seismogenic shallow-dipping normal faults in the Woodlark-D'Entrecasteaux extensional province, Papua New Guinea. *Geology* 19:1205–1208.

Batchelor, G. K. 1967. *An Introduction to Fluid Dynamics*. Cambridge, UK: Cambridge University Press.

Baxter, K., G. T. Cooper, K. C. Hill, and G. W. O'Brian. 1999. Late Jurassic subsidence and passive margin evolution in the Vulcan Sub-basin, north-west Australia: Constraints from basin modelling. *Basin Res*. 11:97–111.

Bertram, G. and N. Milton. 1989. Reconstructing basin evolution from sedimentary thickness: The

importance of palaeobathymetric control, with reference to the North Sea. *Basin Res*. 1:247–257.

Blystad, P., H. Brekke, R. B. Faerseth, B. T. Larson, J. Skogseid, and B. Torudbakken. 1995. *Structural Elements of the Norwegian Continental Shelf*. NPD Bulletin 8. Oslo: Norwegian Petroleum Directorate.

Boillot, G., G. Feraud, M. Recq, and J. Girardeau. 1989a. Undercrusting by serpentinite beneath rifted margins. *Nature* 341:523–525.

Boillot, G., D. Mougenot, J. Girardeau, and E. Winterer. 1989b. Rifting processes on the West Galicia Margin, Spain. In A. Tankard and H. Balkwill, eds., *Extensional Tectonics and Stratigraphy of the North Atlantic Margins*, Memoir, vol. 46, pp. 363–377. Tulsa, OK: American Association of Petroleum Geologists.

Bott, M. and A. Watts. 1970. Deep structure of the continental margin adjacent to the British Isles. In F. Delaney, ed., *The Geology of the East Atlantic Continental Margin*, pp. 89–109. London: British Geological Survey.

Briais, A., P. Patriat, and P. Tapponnier. 1993. Updated interpretation of magnetic anomalies and seafloor spreading stages in the South China Sea: Implications for the Tertiary tectonics of Southeast Asia. *J. Geophys. Res*. 98:6299–6328.

Brodie, J. and N. J. White. 1995. The link between sedimentary basin inversion and igneous underplating. In J. G. Buchanan and P. G. Buchanan, eds., *Basin Inversion*, Special Publication 88, pp. 21–38. London: Geological Society.

Brun, J. P. and M. O. Beslier, 1996. Mantle exhumation at passive margins. *Earth Planet. Sci. Lett*. 142:161–173.

Buck, W. R. 1991. Modes of continental lithospheric extension. *J. Geophys. Res*. 96:20161–20178.

Charpal, O, P. Guennoc, L. Montadert, and D. Roberts. 1978. Rifting, crustal attenuation and subsidence in the Bay of Biscay. *Nature* 275:706–711.

Cheadle, M., S. McGeary, M. Warner, and D. Blundell. 1987. Extensional structures on the western UK continental shelf: a review of deep seismic reflection profiling. In M. Coward, J. Dewey, and P. Hancock, eds., *Continental Extensional Tectonics*, Special Publication 28, pp. 445–465. London: Geological Society.

Chenet, P., L. Montardet, H. Gairaud, and D. Roberts. 1982. Extension ratio measurements on the Galicia, Portugal and Northern Biscay continental margins: Implications for evolutionary models of passive continental margins. In J. S. Watkins and C. L. Drake, eds., *Studies in Continental Margin Geology*, Memoirs, vol. 34, pp. 703–715. Tulsa, OK: American Association of Petroleum Geologists.

Collier, J. S. and A. B. Watts. 1997. Seismic-reflection constraints on lithospheric extension: Pure shear versus simple shear. *Geophys. J. Int*. 129:737–748.

Cook, D. R. 1987. The Goban Spur: Exploration in a deep water frontier basin. In J. Brooks and K. Glennie, eds., *Petroleum Geology of North West Europe*, pp. 623–632. London: Graham and Trotman.

Cordery, M. and J. Phipps-Morgan. 1992. Melting and mantle flow beneath a mid-ocean spreading centre. *Earth Planet. Sci. Lett*. 111:493–516.

Cordoba, D., E. Banda, and J. Ansorge. 1987. The Hercynian crust in northwestern Spain: A seismic survey. *Tectonophysics* 132.

Davis, M. J. 1999. Unpublished Ph.D. thesis, University of Liverpool, UK.

Davis, M. J. and N. J. Kusznir. 2002. Are buoyancy forces important during the formation of rifted margins? *Geophys. J. Int*. 149:524–533.

Decandia, F. and P. Elter. 1969. Riflessioni sul problema delle ophioliti nell'Appennino Settentrionale (Nota preliminare). *Atti Soc. Toscana Sci. Nat.* 76:1–19.

de Graciansky, P. C. and C. W. Poag. 1985. *Site 550, Initial Reports of the DSDP*, vol. 80, pp. 251–289. Washington, DC: U.S. Government Printing Office.

Discovery 215 Working Group (T. A. Minshull, S. Dean, R. B. Whitmarsh, S. Russell, K. E. Louden, and D. Chian). 1998. Deep structure in the vicinity of the ocean-continent transition zone under the southern Iberia Abyssal Plain. *Geology* 26:743–746.

S
N
L

Dore, A. G. and E. R. Lundin. 1996. Cenozoic compressional structures on the NE Atlantic margin: Nature, origin and potential significance for hydrocarbon exploration. *Petroleum Geosci.* 2:299–311.

Dore, A. G., E. R. Lundin, O. Birkeland, P. E. Eliassen, and L. N. Jensen. 1997. The NE Atlantic Margin: Implications of late Mesozoic and Cenozoic events for hydrocarbon prospectivity. *Petroleum Geosci.* 3:117–131.

Driscoll, N. and G. Karner. 1998. Lower crustal extension across the Northern Carnarvon basin, Australia: Evidence for an eastward dipping detachment. *J. Geophys. Res.* 103:4975–4991.

Edwards, P. 1992. Structural evolution of the western Pearl River Mouth Basin. *Mem. Am. Assoc. Petroleum Geol.* 53:43–52.

Eldholm, O., J. Skogseid, S. Planke, and T. P. Gladczenko. 1995. Volcanic margin concepts. In E. Banda, ed., *Rifted Ocean-Continent Boundaries*, pp. 1–16. Dordrecht, The Netherlands: Kluwer.

Gage, M. and A. Dore. 1986. *A Regional Geological Perspective of the Norwegian Offshore Exploration Provinces. Habitat of Hydrocarbons on the Norwegian Continental Shelf*, pp. 21–38. London: Graham and Trotman.

Hall, B. D. and N. J. White. 1994. Origin of anomalous Tertiary subsidence adjacent to North Atlantic continental margins. *Mar. Petroleum Geol.* 11:702–714.

Hinz, K. 1981. A hypothesis on terrestrial catastrophes: wedge of very thick ocean-dipping layers beneath passive continental margins. *Gelo. Jahrb.* (*Ser. E*) 22:3–28.

Horsefield, S. J., R. B. Whitmarsh, R. S. White, and J. C. Sibuet. 1993. Crustal structure of the Goban Spur rifted continental margin, northeast Atlantic. *Geophys. J. Int.* 119:1–19.

Jackson, J. A. 1987. Active normal faulting and crustal extension. In M. P. Coward, J. F. Dewey, and P. L. Hancock, eds., *Continental Extensional Tectonics*, Special Publication 28, pp. 3–18. London: Geological Society.

Jackson, J. A. and D. P. McKenzie. 1983. The geometrical evolution of normal fault systems. *J. Struct. Geol.* 5:236–255.

Jackson, J. A. and D. P. McKenzie. 1988. The relationship between plate motions and seismic moment tensors and the rates of active deformation in the Mediterranean and Middle East. *Geophys. J.* 93:45–73.

Jackson, J., J. Haines, and W. Holt. 1992. The horizontal velocity field in the deforming Aegean Sea region determined from the moment tensors of earthquakes. *J. Geophys. Res.* 97:17657–17684.

Joppen, M. and R. S., White. 1990. The structure and subsidence of Rockall Trough from 2-ship seismic experiments. *J. Geophys. Res.* 95:19821–19837.

Joy, A. M. 1992. Right place, wrong time: Anomalous post-rift subsidence in sedimentary basins around the North Atlantic Ocean. In B. C. Storey, T. Alabaster, and R. J. Pankhurst, eds., *Magmatism and the Causes of Continental Break-up*, Special Publication 68, pp. 387–393. London: Geological Society.

Klemperer, S. and R. Hobbs. 1991. *The BIRPS Atlas: Deep Seismic Reflection Profiles from around the British Isles*. Cambridge, UK: Cambridge University Press.

Kusznir, N. J. 1991. The distribution of stress with depth in the lithosphere: thermo-rheological and geodynamic constraints. *Philos. Trans. R. Soc. Lond. A Math. Phys. Sci. A* 337: 95–110.

Kusznir, N. J. and R. G. Park. 1987. The extensional strength of the continental lithosphere: its dependence on continental gradient, and crustal composition and thickness. In M. P. Coward, J. F. Dewey, and P. L. Hancock, eds., *Continental Extension Tectonics*, Special Publication 28, pp. 35–52. London: Geological Society.

Kusznir, N. J. and P. A. Ziegler. 1992. The mechanics of continental extension and sedimentary basin formation: A simple-shear pure-shear flexural cantilever model. *Tectonophysics* 215:117–131.

Lee, T. Y. and L. A., Lawver. 1994. Cenozoic plate reconstruction of the south china sea region. *Tectonophysics* 235:149–180.

Le Pichon, X. and J. C. Sibuet. 1981. Passive margins: A model of formation. *J. Geophys. Res.* 86:3708–3720.

S
N
L

Lister, G. S., M. A. Etheridge, and P. A. Symonds. 1991. Detachment models for the formation of passive continental margins. *Tectonics* 10:1038–1064.

Louden, K. E., J.-C. Sibuet, and J.-P. Foucher. 1991. Variations in heat flow across the Goban Spur and Galicia continental margins. *J. Geophys. Res*. 96:16131–16150.

Louvel, V., J. Dyment, and J.-C. Sibuet. 1997. Thinning of the Goban Spur continental margin and formation of early oceanic crust: Constraints from forward modelling and inversion of marine magnetic anomalies. *Geophys. J. Int*. 128:188–196.

Manatschal, G. and D. Bernoulli. 1999. Architecture and tectonic evolution of nonvolcanic margins: Present day Galicia and ancient Adria. *Tectonics* 18:1099–1119.

Manatschal, G. and P. Nievergelt. 1997. A continent-ocean transition recorded in the Err and Platta nappes (Eastern Switzerland). *Eclogae Geol. Helv*. 90:3–27.

Marrett, R. and R. W. Allmendinger. 1992. Amount of extension on "small" faults: An example from the Viking Graben. *Geology* 20:47–50.

Marsden, G., A. Roberts, G. Yielding, and N. J. Kusznir. 1990. Application of a flexural cantilever simple-shear/pure-shear model of continental lithosphere extension to the formation of the northern North Sea Basin. *Tectonics of the North Sea Rift*, pp. 240–261. Oxford, UK: Oxford Science Publications.

Masson, D. G., L. Montadert, and R. A. Scrutton. 1985. Evolution of the Goban Spur: History of a starved passive margin. In P. C. de Graciansky and P. C. Poag, eds., *Initial Reports of the DSDP*, vol. 80, pp. 1115–1139. Washington, DC: U.S. Government Printing Office.

Minshull, T. A., S. M. Dean, R. S. White, and R. B. Whitmarsh. 1998. Restricted melting at the onset of seafloor spreading: Ocean-continent transition zones at non-volcanic rifted margins. *Trans. Am. Geophys. Union* 79:906.

McKenzie, D. P. 1978. Some remarks on the development of sedimentary basins. *Earth Planet. Sci. Lett*. 40:25–32.

McKenzie, D. P. 1984. A possible mechanism for epeirogenic uplift. *Nature* 307:616–618.

McKenzie, D. P. and M. J. Bickle. 1988. The volume and composition of melt generated by extension of the lithosphere. *J. Petrol*. 29:625–679.

Mjelde, R., S. Kodaira, P. Digranes, H. Shimamura, T. Kanazawa, H. Shiobara, E. W. Berg, and O. Riise. 1997a. Comparison between a regional and semi-regional crustal OBS model in the Vøring Basin, mid-Norway margin. *Pure Appl. Geophys*. 149:641–665.

Mjelde, R., S. Kodaira, H. Shimamura, T. Kanazawa, H. Shiobara, E. W. Berg, and O. Riise. 1997b. Crustal structure of the central part of the Vøring Basin, mid-Norway margin, from ocean bottom seismographs. *Tectonophysics* 277:235–257.

Mooney, W. and R. Meissner. 1992. Multi-genetic origin of crustal reflectivity: A review. *Dev. Geotectonics* 23:45–79.

Moorcraft, H. and S. Roberts. 1991. *Report of the 1990 CNOOC/BP Joint Study of CA 27/31, Pearl River Mouth Basin, South China Sea.* London: BP Internal Publication.

Murillas, J., D. Mougenot, G. Boillot, M. C. Comas, E. Banda, and A. Mauffret. 1990. Structure and evolution of the Galicia Interior Basin (Atlantic western Iberian continental margin). *Tectonophysics* 184:297–319.

Mutter, J. C., M. Talwani, and P. L. Stoffa. 1982. Origin of seaward dipping reflectors in oceanic crust off the Norwegian margin by "subaerial sea floor spreading." *Geology* 10:353–357.

Nadin, P. and N. J. Kusznir. 1995. Palaeocene uplift and Eocene subsidence in the northern North Sea from 2-D forward and reverse stratigraphic modelling. *J. Geol. Soc. Lond*. 152:833–848.

Nadin, P. A., N. J. Kusznir, and M. J. Cheadle. 1997. Early Tertiary plume uplift of the North Sea and Faeroe-Shetland Basins. *Earth Planet. Sci. Lett.* 148:109–127.

Nissen, S. S., D. E. Hayes, B. C. Yao, W. J. Zeng, Y. Q. Chen, and X. P. Nu. 1995. Gravity, heat-flow, and seismic constraints on the processes of crustal extension: Northern margin of the south-china-sea. *J. Geophys. Res.* 100:22447–22483.

Parsons, B. and J. G. Sclater. 1977. An analysis of the variation of ocean floor bathymetry and heat flow with age. *J. Geophys. Res.* 82:803.

S
N
L

Pautot, G. and C. Rangin. 1989. Subduction of the South China Sea axial ridge below Luzon (Philippines). *Earth Planet. Sci. Lett*. 92:57–69.

Peddy, C., B. Pinet, D. Masson, R. Scrutton, J. C. Sibuet, M. R. Warner, J. P. Lefort, and I. J. Shroeder. 1989. Crustal structure of the Goban Spur continental margin, Northeast Atlantic, from deep seismic reflection profiling. *J. Geol. Soc. Lond*. 146:427–437.

Perez-Gussinye, M., T. Reston, D. Sawyer, C. Ranero, and E. Flueh. 1998. The structure of the Galicia Interior Basin, West of Iberia. *Trans. Am. Geophys. Union* 79:906.

Pickup, S.L.B., R. B. Whitmarsh, C.M.R. Fowler, and T. J. Reston. 1996. Insight into the nature of the ocean-continent transition off West Iberia from a deep multichannel seismic reflection profile. *Geology* 24:1079–1082.

Pitman, W. I. 1978. Relationship between eustasy and stratigraphic sequences of passive margins. *Geol. Soc. Am. Bull*. 89:1389–1403.

Planke, S. and O. Eldholm. 1994. Seismic response and construction of seaward dipping wedges of flood basalts: Vøring volcanic margin. *J.Geophys. Res*. 99:9263–9278.

Reston, T. J. 1996. The S reflector west of Galicia: the seismic signature of a detachment fault. *Geophys. J. Int*. 127:230–244.

Roberts, A. M., N. J. Kusznir, G. Yielding, and P. Styles. 1998. 2D flexural backstripping of extensional basins: The need for a sideways glance. *Petroleum Geosci*. 4:327–338.

Roberts, A., E. R. Lundin, and N. J. Kusznir. 1997. Subsidence of the Vøring Basin and the influence of the Atlantic continental margin: *J. Geol. Soc. Lond*. 154:551–557.

Roberts, A. M., G. Yielding, N. J. Kusznir, I. M. Walker, and D. Dorn-Lopez. 1993. Mesozoic extension in the North Sea: constraints from flexural backstripping, forward modelling and fault populations. In J. R. Parker, ed., *Petroleum Geology of Northwest Europe*, Proceedings of the Fourth Conference, pp. 1123–1136. London: Geological Society of London.

Royden, L. and C. E. Keen. 1980. Rifting process and thermal evolution of the continental margin of Eastern Canada determined from subsidence curves. *Earth Planet. Sci. Lett*. 51:343–361.

Ru, K. and J. D. Pigott. 1986. Episodic rifting and subsidence in the South China Sea. *Bull. Am Assoc. Petroleum Geol*. 70:1136–1155.

Sandwell, D. and W. Smith. 1997. Marine gravity from Geosat and ERS-1 altimetry. *J. Geophys. Res*. 102:10039–10054.

Sclater, J. G. and P.A.F. Christie. 1980. Continental stretching: An explanation of the post mid-Cretaceous subsidence of the central North Sea Basin. *J.Geophys. Res*. 85:3711–3739.

Scrutton, R. A. 1984. Modelling of magnetic and gravity anomalies at Goban Spur, northeast Atlantic. In P. C. de Graciansky and C. W. Poag, eds., *Initial Reports of the Deep Sea Drilling Project 80*. Washington, DC: U.S. Government Printing Office.

Sibuet, J. 1992. Formation of non-volcanic passive margins: A composite model applies to the conjugate Galicia and southeastern Flemish Cap margins. *Geophys. Res. Lett*. 19:769–772.

Spiegelman, N. and D. McKenzie. 1987. Simple 2-D models for melt extraction at mid-ocean ridges and island arcs. *Earth Planet. Sci. Lett*. 83:137–152.

Spiegelman, M. and J. R. Reynolds. 1999. Combined dynamic and geochemical evidence for convergent melt flow beneath the East Pacific Rise. *Nature* 402:282–285.

Stein, R. and S. Barrientos. 1985. Planar high-angle faulting in the Basin and Range: Geodetic analysis of the 1983 Borah Peak, Idaho, earthquake. *J. Geophys. Res*. 90:11355–11366.

Su, D., N. J. White, and D. P. McKenzie. 1989. Extension and subsidence of the Pearl River Mouth Basin, northern South China Sea. *Basin Res*. 2:205–222.

Taylor, B. and D. Hayes. 1983. Origin and history of the South China Basin. In Hayes, D., ed., *Tectonic and geologic evolution of Southeast Asian seas and islands. Geophys. Monogr*. 27:23–56.

Taylor, B. and D. E. Hayes. 1980. The tectonic evolution of the South China basin: The tectonic and geologic evolution of Southeast Asian Seas and Islands. *Geophys. Monogr*. 2:89–104.

Torres, J., S. Bois, and J. Burrus. 1993. Initiation and evolution of the Valencia trough (western Mediterranean): Constraints from deep seismic profiling and subsidence analysis. *Tectonophysics* 228:57–80.

S
N
L

Walsh, J., J. Watterson, and G. Yielding. 1991. The importance of small-scale faulting in regional extension. *Nature* 351:391–393.

Watts, A. B. and J. D. Fairhead, 1997. Gravity anomalies and magmatism along the western continental margin of the British Isles. *J. Geol. Soc*. 154:523–529.

Wernicke, B. 1985. Uniform-sense simple shear of the continental lithosphere. *Can. J. Earth Sci*. 22:108–125.

Westaway, R. 1994. Re-evaluation of extension across the Pearl River Mouth Basin, South China sea: Implications for continental lithosphere deformation mechanisms. *J. Struct. Geol*. 16:823–838.

Westaway, R. and N. Kusznir. 1993. Fault and bed 'rotation' during continental extension: Block rotation or vertical shear? *J. Struct. Geol*. 15:753–770.

White, N. 1990. Does the uniform stretching model work in the North Sea? In D. Blundell and A. Gibbs, eds., *Tectonic Evolution of North Sea Rifts*, pp. 217–239. Oxford, UK: Oxford University Press.

White, N. J. and B. Lovell. 1997. Measuring the pulse of a plume with the sedimentary record. *Nature* 387:888–891.

White, N. J. and D. P. McKenzie. 1988. Formation of the "Steer's Head" geometry of sedimentary basins by differential stretching of the crust and mantle. *Geology* 16:250–253.

White, R. S. and D. McKenzie. 1989. Magmatism at rift zones: The generation of volcanic continental margins and flood basalts. *J. Geophys. Res*. 94:7685–7729.

Whitmarsh, R. B., G. Manatschal, and T. A. Minshull. 2001. Evolution of magma-poor continental margins from rifting to sea-floor spreading. *Nature* 413:150–153.

Whitmarsh, R. B., R. S. White, S. J. Horsefield, J. C. Sibuet, M. Recq, and V. Louvel. 1996. The ocean-continent boundary off the western continental-margin of Iberia: Crustal structure west of Galicia Bank. *J. Geophys. Res*. 101:28291–28314.

S
N
L